'Disorder', structured diffuse scattering and local crystal chemistry

Ray L WITHERS

Research School of Chemistry, Australian National University
Canberra, A.C.T, 0200,
Australia

Abstract

A review of the application of electron microscopy, in particular electron diffraction, to the detection and local structural characterization of 'disordered' materials exhibiting highly structured diffuse intensity distributions is given. A modulation wave approach to structural disorder is taken whereby the observed diffuse distribution is described in terms of what are presumed to be essentially independent, uncorrelated modulation waves, one for each point on the observed diffuse distribution. An equation governing the scattering from such a 'disordered' modulated structure is thereby derived and used to to understand and interpret important qualitative as well as quantitative features of structured diffuse intensity distributions including the notion of transverse and longitudinal polarization, the existence of 'extinction conditions' in diffuse distributions *etc.* The review concludes with some case studies of materials types which typically exhibit highly structured diffuse intensity distributions.

I. INTRODUCTION

The conventional notion of crystalline materials is of essentially perfectly ordered, three-dimensionally (3-d) periodic objects characterized in real space by 3-d unit cells and their atomic contents and in reciprocal space by close to infinitely sharp Bragg reflections falling on the nodes of a corresponding 3-d reciprocal lattice. Whilst this is undoubtedly an excellent approximation for very many materials, a rather large, continually growing and often technologically important family of phases are known where such a description is either inappropriate (*e.g.* long range ordered icosohedral, decagonal or dodecagonal quasicrystalline phases, incommensurate or compositely modulated structures *etc.*; see *e.g.* van Smaalen, 2007; Janssen *et al*, 2007) or grossly inadequate (such as heavily 'disordered' crystalline materials whose reciprocal spaces exhibit highly structured diffuse intensity distributions accompanying the strong Bragg reflections of an underlying average structure, see *e.g.* Fig.1).

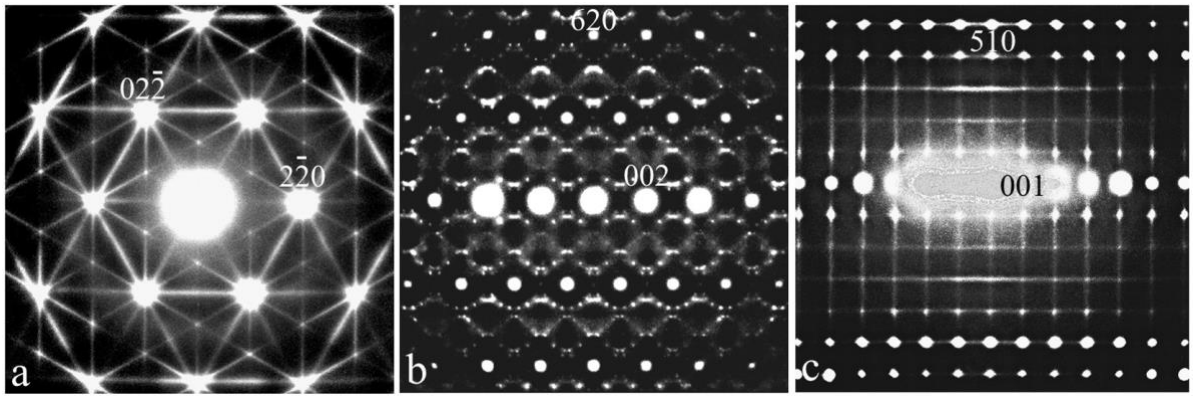

Fig.1 Shows a typical (a) <111> zone axis EDP of β-cristobalite (SiO_2), (b) <-1,3,0> zone axis EDP of 'Sr_2NdNbO_6' and (c) <-1,5,0> zone axis EDP of the relaxor ferroelectric $Ba(Ti_{0.7}Sn_{0.3})TiO_3$. Note the highly structured diffuse intensity distributions accompanying the strong Bragg reflections of the underlying average structure in each case.

'Disordered', or rather locally ordered (as shown by the highly structured diffuse distributions), phases of the latter type are extremely widespread and are the subject matter of this review. Examples (by no means exhaustive) of materials types which exhibit highly structured diffuse intensity distributions at one temperature (or in one polymorphic form) or the other include:

1. A very large number of compositionally 'disordered' solid solution phases *e.g.* (i) the wide range non-stoichiometric (1-x)M^{2+}S.x$Ln_{2x/3}^{3+}$S, *M* = Ca, Mg, Mn, *Ln* = rare earth or Y, solid solution phases (Flahaut, 1979, Withers *et al*, 1994a, 2007), (ii) the widely sub-stoichiometric, transition metal carbide (TC_{1-x}) and nitride (TN_{1-x}) solid solution phases (see *e.g.* Billingham *et al*, 1972, Brunel *et al*, 1972, Sauvage and Parthé, 1972, Anderson, 1984) or (iii) the large family of disordered alloy, and disordered semiconductor alloy, solid solution phases (Sato *et al*, 1962, Ohsima and Watananbe, 1973, Gomyo *et al*, 1988, Matsumura *et al*, 1991) *etc*.

2. Inherently flexible framework structures *e.g.* (i) the ReO_3 or ideal perovskite structure types (Glazer, 1972, Brink *et al*, 2002), (ii) the quartz, cristobalite and tridymite forms of silica, SiO_2, and $AlPO_4$ (van Tendeloo *et al*, 1976, Withers *et al*, 1989, 1994b) or (iii) the large family of zeotypic, microporous molecular sieve materials (Hartmann and Kevan, 1999, Liu *et al*, 2003, Withers and Liu, 2005) *etc*.

3. Materials susceptible to electronic or Fermi surface driven structural instabilities *e.g.* (i) low dimensional materials susceptible to Charge Density Wave (CDW) type instabilities such as the layered transition metal dichalcogenides, the organic charge transfer salts or the non-magnetic Kondo effect materials ThAsSe and UAsSe (Wilson *et al*, 1975, Khanna *et al*, 1977, Withers *et al*, 2006), (ii) certain 'defect' transition metal oxide phases (*e.g.* Castles *et al*, 1971) or (iii) various alloy phases (*e.g.* Norman *et al*, 1985) *etc*.

4. Dynamically disordered, solid electrolyte and related phases *e.g.* (i) $BaTiO_3$, in all but its lowest temperature rhombohedral polymorphic form, and $BaTiO_3$-doped relaxor ferroelectric phases (Comes *et al*, 1968, Harada and Honjo, 1967, Liu *et al*, 2007), (ii) ionic conductors such as *e.g.* α-AgI or γ-$RbAg_4I_5$ (see *e.g.* Andersson *et al*, 1985, Funke and Banhatti, 2006) and the cubic stabilized zirconias (Welberry *et al*, 1995) or (iii) Ag or Cu-containing mineral sulfosalts such as *e.g.* the mineral pearceite (Bindi *et al*, 2006) *etc*.

5. Materials susceptible to ferroelastic strain distortions *e.g.* (i) the tetragonal α form of PbO and $Sn_{1-x}O$ (Withers *et al*, 1993, Withers and Schmid, 1994, Moreno *et al*, 1997), (ii) partially ordered potassium feldspars such as the orthoclase, adularia and intermediate microcline feldspars (McClaren and Fitz Gerald, 1987, Putnis and Salje, 1994) or (iii) the Ni rich, $Ni_{1-x}Al_x$, alloy phase (van Tendeloo and Amelinckx, 1998) and the $In_xGa_{1-x}As_yP_{1-y}$ semiconductor alloy phase (Treacy *et al*, 1985) *etc*.

Significant insight into the local order (and hence the underlying crystal chemistry) of 'disordered' materials of the above types can very often be obtained simply from the 'shapes' of the various structured diffuse intensity distributions characteristic of them (see *e.g.* de Ridder *et al*, 1976a,b, 1977a,b, Withers *et al*, 2007; see also Section IV.A below). Reciprocal space mapping of this type, however, requires a diffraction probe that is sufficiently sensitive to weak features of reciprocal space. Electron diffraction is an ideal such probe as a result of the strength of the interaction between fast electrons and matter. The current paper is thus a review on the application of electron microscopy, in particular electron diffraction, to the detection and characterization of 'disordered'/locally ordered phases. It builds on much earlier pioneering work in the area (see, in particular, Honjo *et al*, 1964, Harada and Honjo, 1967) as well as on many later subsequent reviews (*e.g.* van Tendeloo, 1998, Withers, 2005 *etc.*).

A. *Crystal chemical and other types of flexibility*

A review on 'disordered'/locally ordered phases is simultaneously and inevitably also a review of crystal chemical flexibility and of the numerous ways in which this can be manifested on local, mesoscopic and/or macroscopic length scales (see, for example, Fig.2). A major theme will be that nature, when thoroughly and carefully investigated, often throws up surprises that don't fit into pre-existing categories of how atoms/objects should be arranged and hence, unfortunately, are often neglected or worse ignored! A good example is

the experimental discovery of quasicrystalline materials which began with Dany Shechtman being the first to take seriously electron diffraction patterns (EDP's) exhibiting 'forbidden' symmetries (Shechtman *et al*, 1984) and not accepting the then entrenched conventional wisdom that orientational twinning of conventional 3-d crystalline material somehow had to be responsible (see *e.g.* Pauling, 1985).

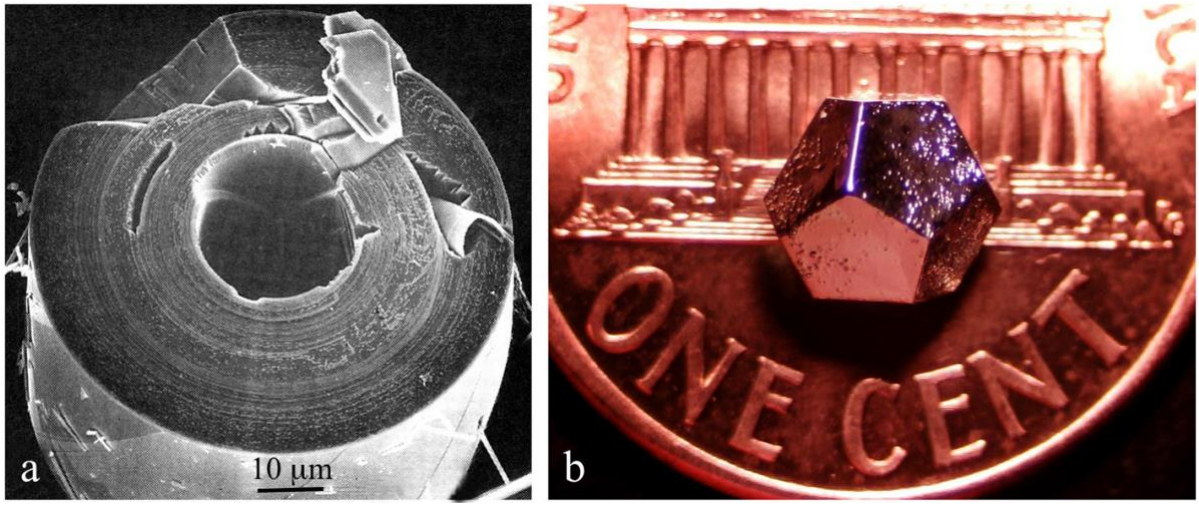

Fig.2 (a) Shows an SEM micrograph of the unusual scroll morphology in which the misfit layer material $Bi_{1.17}Nb_2S_{5.17}$ naturally grows (see Otero-Diaz *et al*, 1995) and (b) an optical micrograph of the perfect dodecahedral symmetry of the mm-sized, single icosahedral quasicrystal $Ho_{8.7}Mg_{34.6}Zn_{56.8}$ (see Fisher *et al*, 2000). Micrographs courtesy of L.C.Otero-Diaz and I.R.Fisher respectively.

Images such as Fig.2b strongly suggest, if not show directly, that large, single phase quasicrystals do indeed exist. In similar vein, the many electron microscopists that inadvertently took images of curved 'graphite' planes and 'onions' in their background holey carbon films in the '60's and '70's but didn't take seriously what that implied may well have missed out on discovering close relatives of buckyballs and buckytubes considerably sooner than they were actually discovered (Kroto *et al*, 1985, Iijima, 1991, Ugarte, 1992 *etc.*)!

While structural science needs systematic categorization, it will also always need flexibility *i.e.* the openness to allow new types of previously unrecognized 'order' to be envisioned, recognized and explored (Mackay, 1976, 1988; Andersson *et al*, 1988; Aragón *et al*, 1993; Klinowski *et al*, 1996; Jacob and Andersson, 1998). What is 'fringe' today is quite

often mainstream tomorrow. A recent (probable) example is the use of a multimetrical (scaling) approach to describe the symmetry and morphology of snow 'crystals' (Janner, 1997) and the later extension of the same idea to biomacromolecules such as nucleic acids with helical structure (Janner, 2001).

An earlier definite example, and one that is central to the current review, was the recognition of long range aperiodic order in (3+*n*)-d modulated structures and the idea of describing them by embedding into higher dimensional 'superspace' rather than attempting to use the (up to then) firmly entrenched notion of 3-d translational symmetry. The notion of aperiodic order was first introduced in a seminal paper of de Wolff (1974) and is nowadays firmly established, including reciprocal space indexation in (3+*n*) dimensions (see *e.g.* Fig.3) as well as systematic listings of higher dimensional superspace group symmetries and their associated systematic extinction conditions (Janssen *et al.*, 1995).

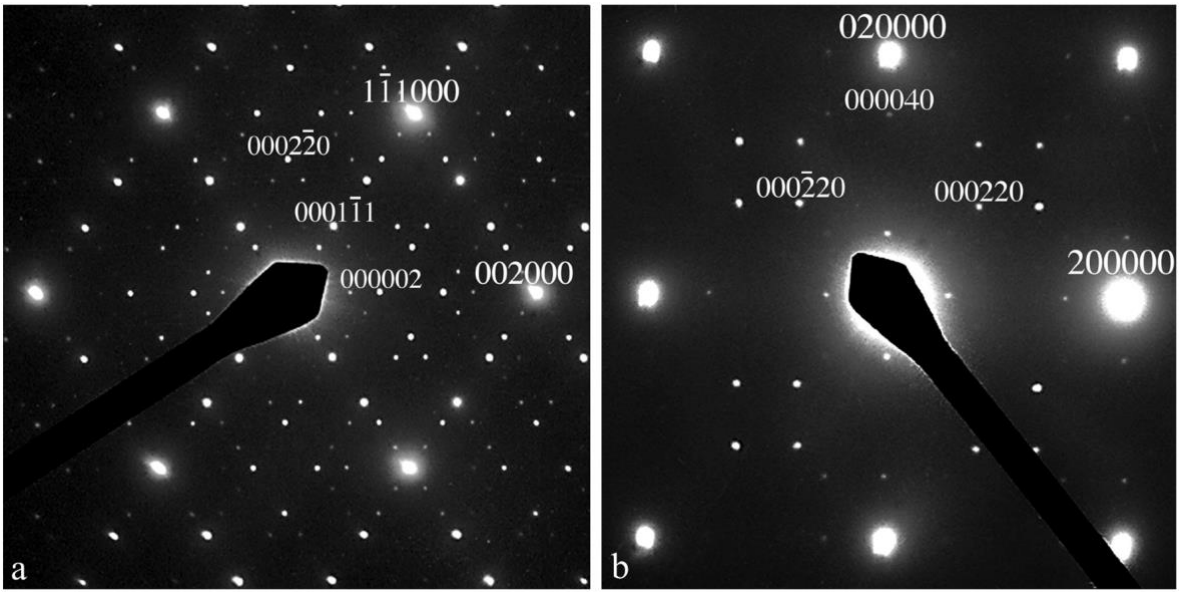

Fig.3 Shows typical (a) <110> and (b) <001> zone axis electron diffraction patterns of the (3+3)-D incommensurately modulated (1-x)Bi_2O_3.xNb_2O_5, $0.06 \leq x \leq 0.25$, solid solution phase for $x \sim 0.2$. Six-dimensional indexation is with respect to the basis vectors **a***, **b***, **c***, $\mathbf{q}_1 = \varepsilon\mathbf{a}^*$, $\mathbf{q}_2 = \varepsilon\mathbf{b}^*$, $\mathbf{q}_3 = \varepsilon\mathbf{c}^*$, $\varepsilon \sim 0.37$ for $x = 0.2$ (see Withers *et al*, 1999 for details).

In the case of the (3+3)-d incommensurately modulated (1-x)Bi_2O_3.xNb_2O_5, $0.06 < x < 0.25$, solid solution phase (Withers *et al*, 1999, Esmaeilzadeh *et al*, 2001), for example, the

characteristic extinction conditions F([*hklmnp*]*) = 0 unless *h*+*k*, *k*+*l*, *h*+*l*, *m*+*n*, *n*+*p*, *m*+*p* are all even and F(<*hk*0*mn*0>*) = 0 unless *m*+*n* = 4J, J an integer (a *d* hyper-glide condition) are clearly observed (see *e.g.* Fig.3). These systematic extinction conditions, in conjunction with the *m*3*m* Laue symmetry of reciprocal space, imply an overall six-dimensional superspace group symmetry of *P*:*Fm3m*:*Fd3m* (in the notation of Yamamoto, 1982). The constraints that such higher dimensional superspace symmetry places upon the Atomic Modulation Functions (AMF's; see *e.g.* Pérez-Mato *et al*, 1987, Janssen *et al*, 1995, van Smaalen, 2007) describing the deviation of any particular long range ordered modulated structure away from its underlying average structure are now generally well understood and encoded into available structure refinement packages such as JANA 2000 (Petricek *et al*, 2000).

The reason that this is of direct relevance to the current paper is that systematic extinction conditions are not only characteristic of long range ordered 3-d or (3+*n*)-d (modulated) structures but also of the structured diffuse intensity distributions characteristic of many so-called 'disordered' materials - see, for example, the [001] zone axis EDP of ThAsSe (average structure space group symmetry *P*4/*nmm*) shown in Fig.4a and the <130> zone axis EDP of $Ca_3CuTi_4O_{12}$, CCTO (average structure space group symmetry *Im*-3) shown in Fig.4b. Note that the **G** ± ~0.14 <110>* ± ε <1,-1,0>* (**G** = [*hkl*]*, ε continuous; *i.e.* the **G** ± ~0.14 [110]* ± ε [1,-1,0]* and **G** ± ~0.14 [1,-1,0]* ± ε [110]*) diffuse 'streaking' in the case of ThAsSe (see Fig.4a) occur only around the *h*+*k* odd, *n*-glide forbidden parent reflections while the diffuse streaking perpendicular to <001> in the case of CCTO (see Fig.4b) only runs through the [*hkl*]*, *l* even parent reflections.

In order to gain insight into the local order hidden in 'disordered' materials of this type it is very helpful, if not essential, to understand the symmetry constraints underlying such extinction conditions and for this the language of modulated structures is ideally suited. The existence of such 'extinction conditions' also suggests the distinct advantages of a modulation

wave approach (Krivoglaz, 1969; de Fontaine, 1972; Pérez-Mato *et al*, 1986, 1987) to the structural description and characterization of 'disordered' materials (Withers, 2005). Such an approach involves describing any observed diffuse distribution in terms of what are presumed to be essentially independent, uncorrelated modulation waves, one for each point on the observed diffuse distribution. An approach of this type automatically emphasizes the close relationship between the crystallography of disordered structures and aperiodic crystallography in general (see *e.g* Perez-Mato *et al*, 1998, Withers, 2005).

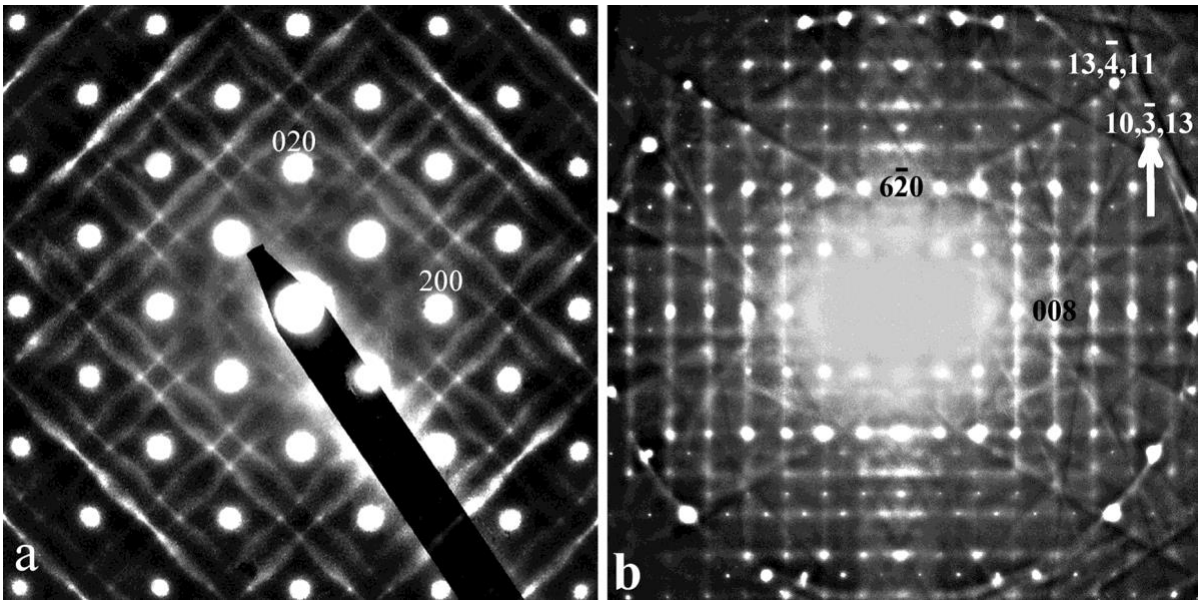

Fig.4 Shows an (a) [001] zone axis EDP of *P*4/*nmm* ThAsSe (see Withers *et al*, 2006 for details) and (b) a <130> zone axis EDP of *Im*-3 CCTO (see Liu *et al*, 2005 for details). Note that the **G** ± ~0.14 <110>* ± ε <1,-1,0>* diffuse 'streaking' in (a) occurs only around the *h*+*k* odd, *n*-glide forbidden parent reflections while the diffuse streaking perpendicular to <001> in (b) only runs through the [*hkl*]*, *l* even parent reflections.

We begin then with a description of the notation used and the derivation of structure factor expressions appropriate for 'disordered' modulated structures. It is assumed in what follows that the modulations giving rise to the observed structured diffuse distribution are of coupled compositional and displacive character. (Note that a sinusoidal compositional modulation with modulation wave-vector **q** will automatically induce a displacive modulation with the same wave-vector). Whilst there are, of course, other types of

modulation possible *e.g.* modulations of magnetic moment or spin state, by far the most common modulated structures are of coupled compositional and/or displacive character.

II. THE MODULATION WAVE APPROACH

In a modulation wave approach (see, for example, Pérez-Mato *et al*, 1986, 1987, Janssen *et al*, 1995 *etc.*), the deviation of the scattering factor of the μ^{th} atom in the average structure unit cell **t** away from its average value can be written in the form

$$\delta f_\mu(\mathbf{r}_\mu+\mathbf{t})/f_\mu^{av} = \Sigma_{\mathbf{q}}\, a_\mu(\mathbf{q})\, \exp[2\pi i \mathbf{q}.(\mathbf{r}_\mu+\mathbf{t})] \quad .. (1)$$

where f_μ^{av} represents the average atomic scattering factor of the μ^{th} atom and $a_\mu(\mathbf{q})$ represents the complex compositional eigenvector associated with the modulation wave-vector **q**, with the property that $a_\mu(-\mathbf{q}) = a_\mu(\mathbf{q})^*$. The displacement of the μ^{th} atom in the unit cell **t** away from its average structure position at $(\mathbf{r}_\mu+\mathbf{t})$ can likewise be written in a similar form as

$$\mathbf{u}_\mu(\mathbf{r}_\mu+\mathbf{t}) = \Sigma_{\mathbf{q}}\, \mathbf{e}_\mu(\mathbf{q})[\exp 2\pi i \mathbf{q}.(\mathbf{r}_\mu+\mathbf{t})]$$
$$= \Sigma_{\mathbf{q}}\, (Re\{\mathbf{e}_\mu(\mathbf{q})\} \cos[2\pi \mathbf{q}.(\mathbf{r}_\mu+\mathbf{t})] - Im\{\mathbf{e}_\mu(\mathbf{q})\} \sin[2\pi \mathbf{q}.(\mathbf{r}_\mu+\mathbf{t})] \quad .. (2)$$

where $\mathbf{e}_\mu(\mathbf{q}) = \Sigma_{\boldsymbol{\alpha}=\mathbf{a},\mathbf{b},\mathbf{c}}\, \boldsymbol{\alpha}\varepsilon_{\mu\alpha}\exp(i\theta_{\mu\alpha})$ represents the complex displacement eigenvector of the μ^{th} atom associated with the modulation wave-vector **q** and has the property that $\mathbf{e}_\mu(-\mathbf{q}) = \mathbf{e}_\mu(\mathbf{q})^*$. Any arbitrary atomic ordering arrangement and/or atomic displacement pattern can then be described in terms of an appropriate summation (over modulation wave-vectors within or on the first Brillouin zone of the underlying average structure) of such compositional and displacive modulation waves (Withers, 2005).

The total scattering amplitude, $F(\mathbf{k})$, from such a 'modulated structure' is given by

$$F(\mathbf{k}) = \Sigma_\mu \Sigma_{\mathbf{t}}\, f_\mu(\mathbf{r}_\mu+\mathbf{t}) \exp\{-2\pi i \mathbf{k}.[(\mathbf{r}_\mu+\mathbf{t})+\mathbf{u}_\mu(\mathbf{r}_\mu+\mathbf{t})]\} \quad .. (3)$$

$$= \Sigma_\mu \Sigma_{\mathbf{t}}\, f_\mu^{av}(1+\Sigma_{\mathbf{q}'}\{a_\mu(\mathbf{q}') \exp[2\pi i \mathbf{q}'.(\mathbf{r}_\mu+\mathbf{t})] + a_\mu(\mathbf{q}')^* \exp[-2\pi i \mathbf{q}'.(\mathbf{r}_\mu+\mathbf{t})]\}) \exp[-2\pi i \mathbf{k}.\mathbf{r}_\mu] \exp[-2\pi i \mathbf{k}.\mathbf{t}] \times$$
$$\Pi_{\mathbf{q}} \exp\{-2\pi i \mathbf{k}.\, (Re\{\mathbf{e}_\mu(\mathbf{q})\} \cos[2\pi \mathbf{q}.(\mathbf{r}_\mu+\mathbf{t})] - Im\{\mathbf{e}_\mu(\mathbf{q})\} \sin[2\pi \mathbf{q}.(\mathbf{r}_\mu+\mathbf{t})])\}$$

(Note that the - sign in the exp{-2πi**k**. ..} factor in Eqn.(3) is not standard crystallographic usage. It is used here, however, to be logically consistent with the use of + signs in the exp [+2πi**k**. ..] factors in Eqns.(1) and (2) above). Then, using the Jacobi-Auger generating relation exp [ixsinθ] = $\Sigma_m J_m(x)$ exp [imθ], where the summation over the integer m is from - ¥ to + ¥ and the J_m are m^{th} order Bessel functions,

$$F(\mathbf{k}) = \Sigma_\mu \Sigma_{\mathbf{t}} f_\mu^{av}(1+\Sigma_{\mathbf{q}'} \{a_\mu(\mathbf{q}') \exp[2\pi i\mathbf{q}'.(\mathbf{r}_\mu+\mathbf{t})] + a_\mu(\mathbf{q}')^* \exp[-2\pi i\mathbf{q}'.(\mathbf{r}_\mu+\mathbf{t})]\}) \exp[-2\pi i\mathbf{k}.\mathbf{r}_\mu] \exp[-2\pi i\mathbf{k}.\mathbf{t}]$$

$$\times \Pi_{\mathbf{q}} \Sigma_{m,m'} J_m[2\pi\mathbf{k}.(Re\{\mathbf{e}_\mu(\mathbf{q})\})] \exp im[2\pi\mathbf{q}.(\mathbf{r}_\mu+\mathbf{t}) - \pi/2] J_{m'}[2\pi\mathbf{k}.(Im\{\mathbf{e}_\mu(\mathbf{q})\})] \exp im'[2\pi\mathbf{q}.(\mathbf{r}_\mu+\mathbf{t})]$$

$$= \Sigma_\mu \Sigma_{\mathbf{t}} f_\mu^{av} \exp[-2\pi i\mathbf{k}.\mathbf{r}_\mu] \exp[-2\pi i\mathbf{k}.\mathbf{t}] (1+\Sigma_{\mathbf{q}'} \{a_\mu(\mathbf{q}') \exp[2\pi i\mathbf{q}'.(\mathbf{r}_\mu+\mathbf{t})] + a_\mu(\mathbf{q}')^* \exp[-2\pi i\mathbf{q}'.(\mathbf{r}_\mu+\mathbf{t})]\})$$

$$\times \Pi_{\mathbf{q}} \Sigma_{m,m'} J_m(2\pi\mathbf{k}.(Re\{\mathbf{e}_\mu(\mathbf{q})\}) J_{m'}(2\pi\mathbf{k}.(Im\{\mathbf{e}_\mu(\mathbf{q})\}) \exp[-im\pi/2] \exp[i(m+m')2\pi\mathbf{q}.(\mathbf{r}_\mu+\mathbf{t})]$$

At this stage, reasonable approximations need to be made in order to simplify the above general expression into a more tractable, and hence useful, form. The question is, what possible approximations are reasonable and what are not? In Fig.4a, note that only the first order harmonic **G** ± **q** (**G** a Bravais lattice allowed, average structure Bragg reflection and **q** = ~ 0.14 <110>* ± ε <1,-1,0>*, ε continuous) primary 'reflections' constituting the continuous 'primary' diffuse streaking are visible *i.e.* no second harmonic copy of the primary diffuse distribution is visible. The same is also true of the more complex curved primary diffuse distribution shown in Fig.5b.

Such observations strongly suggest that there is almost invariably never any correlation between the different individual 'primary modulation wave-vectors' constituting the primary diffuse distribution, in distinction to what is clearly the case for a conventional (3+*n*)-d (*n* > 1) incommensurately modulated structure (see *e.g.* Fig.3 where higher order harmonic satellite reflections are clearly present). Thus, in almost all cases, an eminently reasonable assumption is that the generally weak, primary diffuse distribution at **G** ± **q**, arises solely from compositional and/or displacive modulation waves associated with the different individual primary modulation wave-vectors **q**.

In Fig.5a, however, note that the primary modulation wave-vectors **q** = ~0.49 <100>* ± <0, 0.245, γ>* (γ continuous, see Brink *et al*, 2004 for the details) constituting the primary diffuse streaking are accompanied by a very much weaker (indeed mostly barely visible), second order harmonic 2**q** = ~0.98 <100>* ± <0, 0.489, γ>* secondary diffuse streaking (arrowed at the bottom of Fig.5a).

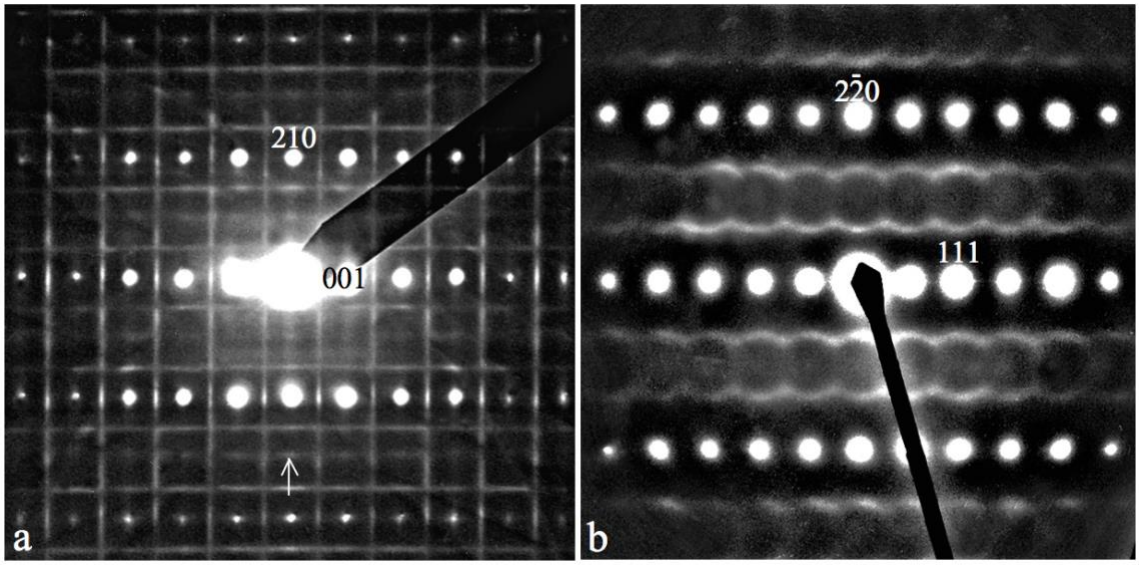

Fig.5 Shows an (a) <-1,2,0> zone axis EDP of $Nb^{V}_{0.52}Nb^{IV}_{0.48}O_{1.52}F_{1.48}$ (see Brink *et al*., 2004 for details) and (b) a <1,1,-2> zone axis EDP characteristic of the (1-*x*)CaS.*x*Y_2S_3, $0 < x < 0.29$, solid solution at $x = {}^{2}/_{7}$ (indexed with respect to the underlying *NaCl*-type average structure, see Withers *et al.*, 1994a for details).

This suggests that, for completeness, the above assumption (that the primary diffuse distribution at **G** ± **q** arises solely from modulation waves associated with the different individual primary modulation wave-vectors **q**) may need, in some inherently more anharmonic cases (see *e.g.* Brink *et al*, 2002), to be supplemented by the addition of necessarily small amplitude compositional and/or displacive modulation waves associated with the second harmonic modulation wave-vectors 2**q**.

Under these approximations, the above expression simplifies to

$$F(\mathbf{k}) = \Sigma_{\mathbf{q}} \Sigma_{\mu} \Sigma_{m,m',n,n'} f_{\mu}^{av} \exp[-i(m+n)\,\pi/2] \exp\{-2\pi i[\mathbf{k}-(m+m')\mathbf{q}-(n+n')2\mathbf{q}].\mathbf{r}_{\mu}\}$$
$$J_m(2\pi\mathbf{k}.(Re\{\mathbf{e}_{\mu}(\mathbf{q})\})\, J_{m'}(2\pi\mathbf{k}.(Im\{\mathbf{e}_{\mu}(\mathbf{q})\}) \times J_n(2\pi\mathbf{k}.(Re\{\mathbf{e}_{\mu}(2\mathbf{q})\})\, J_{n'}(2\pi\mathbf{k}.(Im\{\mathbf{e}_{\mu}(2\mathbf{q})\})$$
$$\Sigma_{\mathbf{t}}\{\exp(-2\pi i[\mathbf{k}-(m+m')\mathbf{q}-(n+n')2\mathbf{q}].\mathbf{t})$$

$+ a_\mu(\mathbf{q}) \exp[2\pi i \mathbf{q}.\mathbf{r}_\mu] \exp(-2\pi i[\mathbf{k}-\mathbf{q}-(m+m')\mathbf{q}-(n+n')2\mathbf{q}].\mathbf{t}) + a_\mu(\mathbf{q})^* \exp[-2\pi i \mathbf{q}.\mathbf{r}_\mu] \exp(-2\pi i[\mathbf{k}+\mathbf{q}-(m+m')\mathbf{q}-(n+n')2\mathbf{q}].\mathbf{t})$

$+ a_\mu(2\mathbf{q}) \exp[4\pi i \mathbf{q}.\mathbf{r}_\mu] \exp(-2\pi i[\mathbf{k}-2\mathbf{q}-(m+m')\mathbf{q}-(n+n')2\mathbf{q}].\mathbf{t}) + a_\mu(2\mathbf{q})^* \exp[-4\pi i \mathbf{q}.\mathbf{r}_\mu] \exp(-2\pi i[\mathbf{k}+2\mathbf{q}-(m+m')\mathbf{q}-(n+n')2\mathbf{q}].\mathbf{t})\}$

$$= N \Sigma_{\mathbf{q}'} \Sigma_\mu \Sigma_{m,m',n,n'} f_\mu^{av} \exp[-i(m+n)\,\pi/2] \exp\{-2\pi i[\mathbf{k}-(m+m')\mathbf{q}-(n+n')2\mathbf{q}].\mathbf{r}_\mu\} \times$$

$$J_m(2\pi\mathbf{k}.(Re\{\mathbf{e}_\mu(\mathbf{q})\}) J_{m'}(2\pi\mathbf{k}.(Im\{\mathbf{e}_\mu(\mathbf{q})\}) \times J_n(2\pi\mathbf{k}.(Re\{\mathbf{e}_\mu(2\mathbf{q})\}) J_{n'}(2\pi\mathbf{k}.(Im\{\mathbf{e}_\mu(2\mathbf{q})\}) \times$$

$$\Sigma_{\mathbf{G}}\{\delta([\mathbf{k}-(m+m')\mathbf{q}-(n+n')2\mathbf{q}]-\mathbf{G})$$

$+ a_\mu(\mathbf{q}) \exp[2\pi i \mathbf{q}.\mathbf{r}_\mu] \delta([\mathbf{k}-\mathbf{q}-(m+m')\mathbf{q}-(n+n')2\mathbf{q}]-\mathbf{G}) + a_\mu(\mathbf{q})^* \exp[-2\pi i \mathbf{q}.\mathbf{r}_\mu] \delta([\mathbf{k}+\mathbf{q}-(m+m')\mathbf{q}-(n+n')2\mathbf{q}]-\mathbf{G})$

$+ a_\mu(2\mathbf{q}) \exp[4\pi i \mathbf{q}.\mathbf{r}_\mu] \delta([\mathbf{k}-2\mathbf{q}-(m+m')\mathbf{q}-(n+n')2\mathbf{q}]-\mathbf{G}) + a_\mu(2\mathbf{q})^* \exp[-4\pi i \mathbf{q}.\mathbf{r}_\mu] \delta([\mathbf{k}+2\mathbf{q}-(m+m')\mathbf{q}-(n+n')2\mathbf{q}]-\mathbf{G})\}$ .. (4)

Note that the second order modulation wave amplitudes associated with the individual secondary modulation wave-vectors, $2\mathbf{q}$, must necessarily each have small amplitudes so that diffuse intensity is either not observed, or only very weakly observed, at the $\mathbf{G} \pm 2\mathbf{q}$ positions of reciprocal space (to be consistent with the observed experimental diffraction evidence, see *e.g.* Fig.4a and Fig.5). For the purposes of this derivation, the modulation wave amplitudes $a_\mu(2\mathbf{q})$ and $\mathbf{e}_\mu(2\mathbf{q})$ were thus treated as being of second order with respect to the already weak primary modulation wave amplitudes $a_\mu(\mathbf{q})$ and $\mathbf{e}_\mu(\mathbf{q})$ respectively.

Given that the observed intensity at $(\mathbf{G} \pm 2\mathbf{q})$ is either zero or very weak in most cases and that $F(\mathbf{k} = \mathbf{G} + 2\mathbf{q}) = N\Sigma_\mu f_\mu^{av} \exp[-2\pi i \mathbf{G}.\mathbf{r}_\mu] \times \{a_\mu(2\mathbf{q}) - {}^{i}/_{2}\,(2\pi[\mathbf{G}+2\mathbf{q}].\mathbf{e}_\mu(2\mathbf{q}))$ $-{}^{1}/_{8}(2\pi[\mathbf{G}+2\mathbf{q}].\mathbf{e}_\mu(\mathbf{q}))^2 - {}^{i}/_{2}\, a_\mu(\mathbf{q}) \times (2\pi[\mathbf{G}+2\mathbf{q}].\mathbf{e}_\mu(\mathbf{q}) + ..\}$ (from substitution into Eqn.(4) above), corresponding to a fourth order contribution (in terms of $a_\mu(\mathbf{q})$ and $\mathbf{e}_\mu(\mathbf{q})$) to the intensity at $(\mathbf{G} + 2\mathbf{q})$, it is logical to only include up to third order terms in a Taylor series type expansion of $F(\mathbf{k} = \mathbf{G} + \mathbf{q})$. Expanding Eqn.(4) above for $F(\mathbf{k} = \mathbf{G} + \mathbf{q})$ up to third order in the modulation wave eigenvectors $a_\mu(\mathbf{q})$ and $\mathbf{e}_\mu(\mathbf{q})$ then leads to the final structure factor expression

$$F(\mathbf{k} = \mathbf{G} + \mathbf{q}) = N\Sigma_\mu f_\mu^{av} \exp[-2\pi i \mathbf{G}.\mathbf{r}_\mu] \times \{a_\mu(\mathbf{q}) - {}^{i}/_{2} \times 2\pi[\mathbf{G}+\mathbf{q}].\mathbf{e}_\mu(\mathbf{q})$$

$$- {}^{1}/_{4}\, a_\mu(\mathbf{q}) |2\pi[\mathbf{G}+\mathbf{q}].\mathbf{e}_\mu(\mathbf{q})|^2 + {}^{i}/_{16} |2\pi[\mathbf{G}+\mathbf{q}].\mathbf{e}_\mu(\mathbf{q})|^2 \times (2\pi[\mathbf{G}+\mathbf{q}].\mathbf{e}_\mu(\mathbf{q})) - {}^{1}/_{8}\, a_\mu(\mathbf{q})^* (2\pi[\mathbf{G}+\mathbf{q}].\mathbf{e}_\mu(\mathbf{q}))^2$$

$$- {}^{1}/_{4}\, (2\pi[\mathbf{G}+\mathbf{q}].\mathbf{e}_\mu(\mathbf{q})^*) \times (2\pi[\mathbf{G}+\mathbf{q}].\mathbf{e}_\mu(2\mathbf{q})) - {}^{i}/_{2}\, a_\mu(2\mathbf{q})\, (2\pi[\mathbf{G}+\mathbf{q}].\mathbf{e}_\mu(\mathbf{q})^*) ..\} \text{ .. (5)}$$

This is the fundamental equation governing the scattering from a 'disordered' modulated structure and will be used throughout this review to understand and interpret important

qualitative as well as quantitative features of structured diffuse intensity distributions. In most instances described below, however, it will only be necessary to include the expansion in Eqn.(5) up to first order *i.e.* only including the first line of the above expression.

III. APPPLICATIONS OF THE MODULATION WAVE APPROACH

III.A *Transverse and Longitudinal Polarization*

Given the above structure factor expression, there are a number of qualitative, but nonetheless very important, conclusions that can often be drawn from experimental electron diffraction patterns (EDP's). When, for example, strong azimuthal (angular) variation in the intensity of an observed diffuse distribution occurs (see *e.g.* the [001] zone axis EDP of ThAsSe shown in Fig.4a or the [130] zone axis EDP of $CaCu_3Ti_4O_{12}$ (CCTO) in Fig.4b (particularly at large **G** towards the edges of these patterns, where the relative contribution of the first order displacive to compositional component of the structure factor $F(\mathbf{k} = \mathbf{G} + \mathbf{q})$ is significantly enhanced and where the effects of multiple scattering are much reduced), then the major contribution to the observed diffuse intensity necessarily arises from displacive disorder. (Note, however, that this does not mean that the observed distribution cannot have a compositional origin; see, for example, Brink *et al*, 2002). Furthermore, the relationship between the displacement eigenvector of the most heavily displaced atom/s, $\mathbf{e}_\mu(\mathbf{q})$, and the modulation wave-vector itself, **q**, can be readily deduced (see *e.g.* Fig.6 below).

If $\mathbf{e}_\mu(\mathbf{q})$ is, for example, perpendicular to **q**, the modulation is said to be transverse polarized (in just the same way as an electromagnetic wave is transverse polarized because the fluctuating electric and/or magnetic field direction involved in an electromagnetic wave is perpendicular, or transverse, to the wave direction itself; see *e.g.* Fig.6a) while the modulation is said to be longitudinally polarized if $\mathbf{e}_\mu(\mathbf{q})$ is parallel to **q** (in just the same way

as a sound wave is longitudinally polarized because the fluctuating pressure or density wave involved in a sound wave is parallel to the wave direction itself, see *e.g.* Fig.6b).

Note that $F(\mathbf{G} + \mathbf{q})$ is experimentally zero whenever $(\mathbf{G} + \mathbf{q})$ is perpendicular to $\mathbf{e}_\mu(\mathbf{q})$ in Fig.6 (*i.e.* along the vertical direction in Fig.6a and along the horizontal direction in Fig.6b). This is a direct consequence of the structure factor expression given in Eqn.(5) above in that $F_\mu(\mathbf{G} + \mathbf{q}) \alpha 2\pi[\mathbf{G}+\mathbf{q}].\mathbf{e}_\mu(\mathbf{q})$ and clearly goes to zero whenever $(\mathbf{G} + \mathbf{q})$ is perpendicular to $\mathbf{e}_\mu(\mathbf{q})$, just as the calculated diffraction patterns on the right hand side of Fig.6 show.

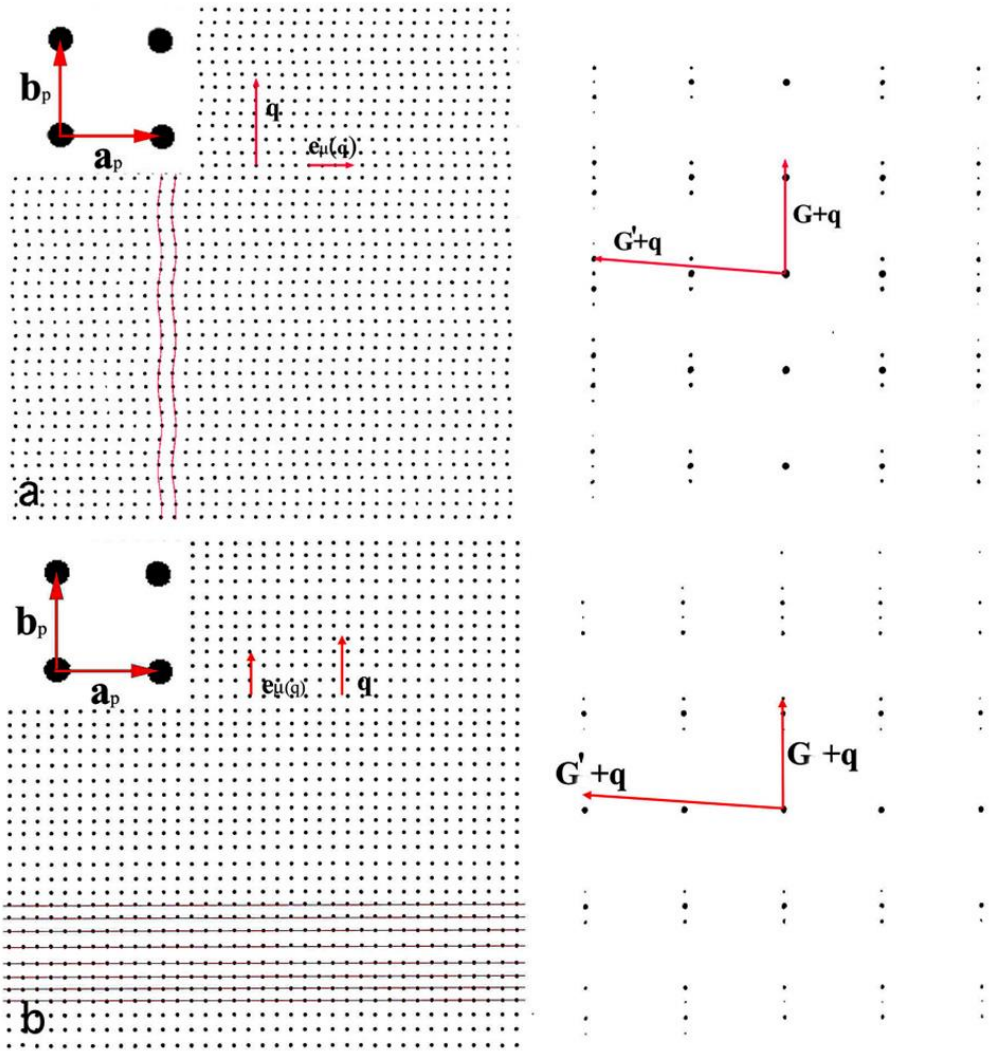

Fig.6 Shows an (a) transverse modulated (*i.e.* $\mathbf{e}_\mu(\mathbf{q})$ perpendicular to $\mathbf{q}$) square, single atom array on the left and its corresponding diffraction pattern on the right and (b) a longitudinally modulated (*i.e.* $\mathbf{e}_\mu(\mathbf{q})$ parallel to $\mathbf{q}$) square, single atom array on the left and its corresponding diffraction pattern on

the right. The modulation wave-vector **q** is the same in both (a) and (b). Permission to reproduce the figure from F.J.Brink. Adapted from Harburn *et al*, 1975.

The same type of resultant reciprocal space intensity distribution will of course hold true when **q** is not an isolated individual primary modulation wave-vector (as in Fig.6) but rather part of an essentially continuous diffuse intensity distribution (as in Fig.4). Thus the **G** ± ~0.14 <110>* ± ε <1,-1,0>* (ε continuous) 'lines' of diffuse streaking (running along the [1,-1,0]* and [110]* directions of reciprocal space respectively around the nominally *n* glide forbidden *hk*0, *h*+*k* odd reflections) in Fig.4a necessarily arise from transverse polarized, [110] and [1,-1,0] displacements, respectively (for further details, see Withers *et al*, 2004). Likewise, the strong transverse polarized, azimuthal intensity variation of the characteristic diffuse streaking running perpendicular to **c*** through the *hkl*, *l* even Bragg reflections of CCTO in Fig.4b requires the atomic displacements responsible to run perpendicular to the diffuse streaking itself *i.e.* along the [001] direction (for more details, see Liu *et al*, 2005).

III.B "*Extinction Conditions*"

The structure factor expression given in Eqn.(5) also provides the basis for understanding the existence of 'extinction conditions' in experimentally observed diffuse distributions, both symmetry induced as well as accidental (see *e.g.* Withers, 2005).

Consider, for example, the [130] zone axis EDP of CCTO shown in Fig.4b. Note the **G** ± ε[6,-2,0]* (ε continuous) diffuse streaking which only runs through the **G** = [*hkl*]*, *l* even, parent reflections to a very good approximation. (Similar <*uv*0> type zone axis EDP's to Fig.4b [Liu *et al*, 2005] show that this **q** = ε[6,-2,0]* diffuse streaking is only a part of essentially continuous (001)* sheets of diffuse intensity running through the [*hkl*]*, *l* even but not *l* odd, parent reflections). Note furthermore that the intensity of this **G** ± ε[6,-2,0]* diffuse streaking in Fig.4b goes precisely to zero along the exact **G =** [6,-2,0]* direction of reciprocal space itself.

As discussed in Section III.A above, this observation requires that the atomic displacements responsible for the diffuse streaking in Fig.4b and the overall {001}* sheets of diffuse intensity necessarily run along the <001> real space directions (see *e.g.* the Ti shifts arrowed in Fig.7b). Finally note that the diffuse streaking disappears altogether at the exact <001> zone axis orientation (see Fig.7a).

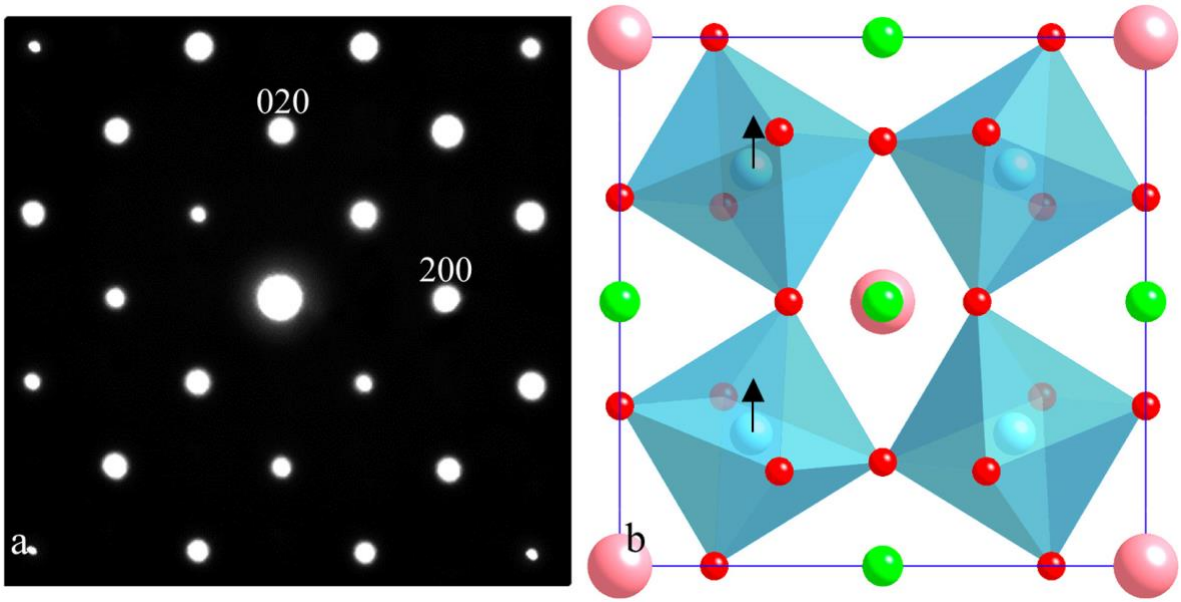

Fig.7 Shows an (a) <001> zone axis EDP of *Im*-3, $Ca_3CuTi_4O_{12}$ (CCTO). Note the complete absence of diffuse streaking at this zone axis orientation orientation. (b) shows a unit cell of the *Im*-3, CCTO average structure in projection along a <100> direction. The corner-connected TiO_6 octahedra are shown in blue, the Ca ions are represented by the large pink balls, the Ti and Cu ions by the medium sized blue and green balls respectively and the O ions by the small red balls. The black arrows show the correlated Ti shifts along one of the <001> directions (correlated along this particular <001> row direction but not from one such <001> to the next) responsible for the structured diffuse scattering observed in Fig.4b.

How can we rationalize/understand these experimental observations? First of all, CCTO has a non-polar, average structure space group symmetry of *Im*-3 (shown in Fig.7b). Now imagine breaking the observed (001)* sheet of diffuse intensity into individual modulation waves characterized by modulation wave-vectors of the type $\mathbf{q} = \alpha\mathbf{a}^* + \beta\mathbf{b}^*$ and then treating each of these primary modulation waves as completely independent of one another, just as described in Section II above. The structural description problem then

becomes effectively equivalent to dealing with a series of uncoupled or independent (3+1)-d incommensurately modulated structures (IMS's), one for each modulation wave-vector making up the observed (001)* sheet of diffuse intensity.

For each of these individual IMS's, there are only two symmetry operations of the parent *m*-3 point group symmetry that map the associated $\mathbf{q} = \alpha\mathbf{a}^* + \beta\mathbf{b}^*$ into itself, the identity *E* and reflection in a mirror plane perpendicular to **c** *i.e.* m_z. The so-called little co-group of a general such modulation wave-vector G^q is then = {*E*, m_z} (see *e.g.* Bradley and Cracknell, 1972). There are only two possible irreducible representations (*irreps*) associated with such a modulation wave-vector, the totally symmetric representation and a second *irrep* with a character of -1 under the parent symmetry operation $\{m_z|\mathbf{0}\}$. For satellite reflections of the type [*hk*0]* + **q** to be symmetry forbidden (and hence missing from EDP's such as Figs.7a and 4b), all that is required is that the *irrep* associated with each individual modulation wave-vector $\mathbf{q} = \alpha\mathbf{a}^* + \beta\mathbf{b}^*$ (making up the overall (001)* sheet of diffuse intensity) transforms according to this second *irrep*.

An alternative, but equivalent, way to state the same thing is to say that the (3+1)-d superspace group symmetry associated with any individual IMS should be *I*112/*m* (α,β,0)0s (a non-standard setting of the superspace group *B*112/*m* (α,β,0)0s, Number 12.2 in Table 9.8.3.3.5 of Janssen *et al*, 2005). In addition to the centreing condition F(*hklm*) = 0 unless *h*+*k*+*l* is even, this superspace group also ensures that F(*hk*0*m*) = 0 for *m* = 1, just as is required and observed experimentally (see Fig.4b and Fig.7a).

This then explains the absence of diffuse intensity in the [001] zone axis EDP of Fig.7a. It does not, however, explain the fact that the $\mathbf{G} \pm \varepsilon$[6,-2,0]* diffuse streaking in Fig.4b only runs through the [*hkl*]*, *l* even (and not *l* odd) parent reflections. To understand this, it is necessary to return to the first order displacive form of Eqn.(5) *i.e.* to the expression

$$F(\mathbf{G}+\mathbf{q}) = N\Sigma_\mu f_\mu \exp[-2\pi i \mathbf{G}.\mathbf{r}_\mu] \times \{-^{i}/_{2}\,(2\pi[\mathbf{G}+\mathbf{q}].\mathbf{e}_\mu(\mathbf{q}))\}$$

From the mathematical form of this structure factor expression, it is apparent that the observed $F([hkl]^* + [\alpha\beta0]^*) = 0$ unless l is odd, pseudo-extinction condition (see *e.g.* Fig.4b) requires the displacement eigenvectors, $\mathbf{e}_\mu(\mathbf{q} = [\alpha\beta0]^*)$, of two atoms separated by $^1/_2$ **c** to displace by the same amount along the **c** axis. The only candidate atoms which can satisfy this requirement are the Ti atoms (see *e.g.* Fig.7b). Consider, for example, two such Ti atoms - Ti1 at $\mathbf{r}_{Ti1} = [^1/_4, ^1/_4, ^1/_4]$ and Ti2 at $\mathbf{r}_{Ti2} = [^1/_4, ^1/_4, ^3/_4]$. Suppose that $\mathbf{e}_{Ti2}$ (at $\mathbf{r}_{Ti2} = [^1/_4, ^1/_4, ^3/_4]$) = + $\mathbf{e}_{Ti1}$ (at $\mathbf{r}_{Ti1} = [^1/_4, ^1/_4, ^1/_4]$) = $e_{Ti}\mathbf{c}$ for all $\mathbf{q} = [\alpha\beta0]^*$. Substitution into the above expression shows that

$$F(\mathbf{G}+\mathbf{q}) \alpha \exp[-i\pi(h+k+l)/2]\{1 + \exp[-i\pi l]\} \times (2\pi[\mathbf{G}+\mathbf{q}].\, e_{Ti}\mathbf{c}\,(\mathbf{q})) = 0 \text{ unless } l \text{ is even.}$$

There are four such pairs of Ti atoms per parent unit cell (see Fig.7b). Provided the atoms in each pair obey the constraint that they displace by the same amount along **c**, the Ti contribution to the observed extinction condition will continue to be obeyed. On the other hand, if the Ca, Cu or O atoms displaced in a similar correlated fashion, then the observed extinction condition would no longer be obeyed. Likewise, if the Ti atoms displaced perpendicular to **c** in opposite directions (as allowed by the second *irrep*) in a correlated fashion, then the observed extinction condition would again no longer be obeyed. Thus the observation of this well-obeyed (see *e.g.* Fig.4b) 'extinction condition' not only allows us to determine that $\mathbf{e}_{Ti2} = + \mathbf{e}_{Ti1} = e_{Ti}\mathbf{c}$ for all $\mathbf{q} = [\alpha\beta0]^*$ but also that the Ca, Cu and O ions do not displace at all.

In the case of CCTO, this is of some interest as these <001> displacements of the Ti ions (correlated along the <001> directions themselves but uncorrelated from any one such column to the next in the transverse direction) effectively set up 1-d dipole moments and show that CCTO is an incipient ferroelectric (Liu *et al*, 2005). The existence of 'extinction conditions' (whether absolute in symmetry terms or not) in diffuse distributions can thus

clearly provide great insight into the origin of the structural disorder responsible (whether static or dynamic in origin, see *e.g.* Aroyo *et al*, 2002a,b, Perez-Mato *et al*, 1998, van Tendeloo, 1998). It also emphasizes the links between 'disorder' and the crystallography of modulated structures. In certain favourable cases, as seen above, it is even possible to virtually solve for the real space origin of an observed diffuse distribution from such 'extinction conditions'.

III.C ***Planar diffuse absences***

Apparent extinction conditions in diffuse distributions can, however, also arise for other reasons. It is surprisingly often the case, for example, that a highly structured diffuse intensity distribution is clearly visible when tilted only slightly away from some major zone axis orientation but disappears entirely when one tilts to the exact zone axis orientation (see *e.g.* Fig.8; see also Welberry, 1986, Liu *et al*, 2003, Butler *et al*, 1992 *etc.*).

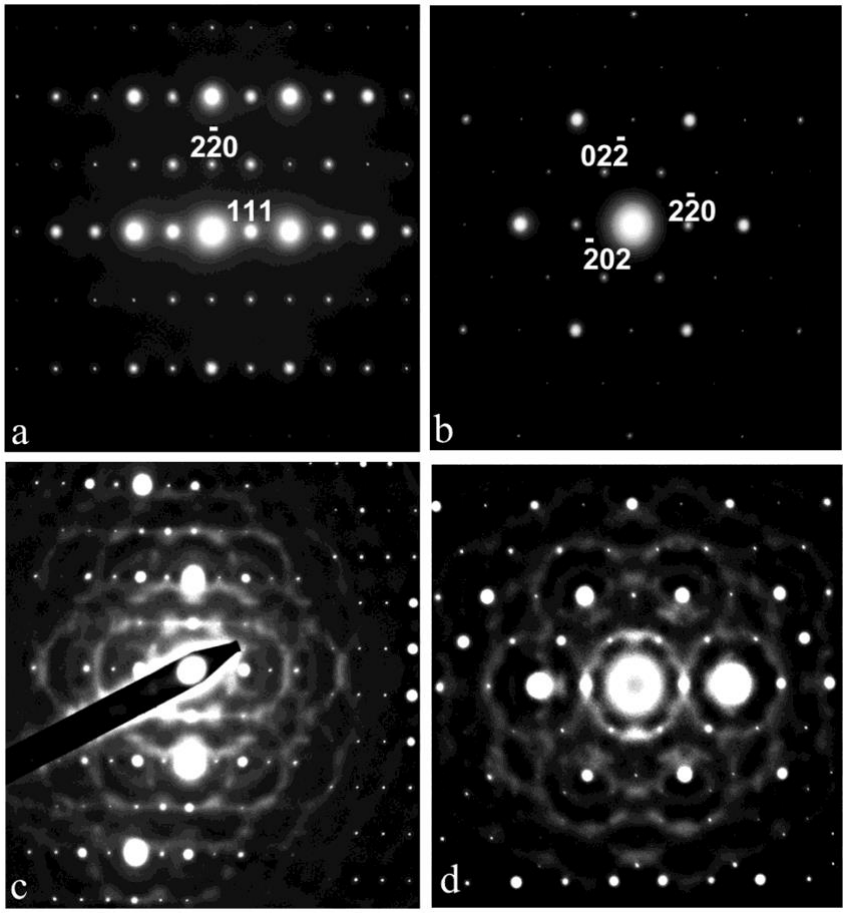

Fig.8 Shows (a) [1,1,-2] and (b) [111] zone axis EDP's of the disordered *Fd*-3*m*, Bi-based pyrochlore $Bi_{1.89}GaSbO_{6.84}$ (see Ismunandar *et al*, 1999 for details of the average structure). Note the complete absence of diffuse streaking in either EDP at the exact zone axis orientation. EDP's taken tilted only a few degrees away from the exact [1,1,-2] and [111] zone axis orientations are shown in (c) and (d) respectively.

While the absence of diffuse intensity in the <001> zone axis EDP of CCTO in Fig.7a (as well as the hyper-glide plane type extinction condition exhibited by the diffuse distribution in Fig.4a, see Withers *et al*, 2006) can be explained in terms of superspace symmetry arguments (as outlined in Section II.B above), the same can not be true for the [1,1,-2] and [111] zone axis EDP's of $Bi_{1.89}GaSbO_{6.84}$ shown in Fig.8.

The reason is that the average structure space group symmetry of this disordered pyrochlore is *Fd*-3*m* (Ismunandar *et al*, 1999) and hence there is no mirror plane perpendicular to either [1,1,-2] or [111] in reciprocal space *i.e.* the little co-group of a general modulation wave-vector in the Zero Order Laue Zones of Fig.8a or b consists only of the identity operation. The sudden disappearance of the structured diffuse scattering at the exact zone axis orientations in Fig.8 can not therefore be attributed to any symmetry condition. Rather such planar diffuse absences require that there is simply no modulation (either compositional and/or displacive) when one projects down the exact zone axis orientations.

Why should this be the case? The most likely explanation is that it avoids energetically costly macroscopic strain along the polyhedrally closest-connected <110>, <112> and <111> directions (see Fig.9 below). Any compositional modulation (*e.g.* of the occupancy of the O' ions in the red $O'Bi_4$ tetrahedra or of the relative Ga/Sb occupancy of the green $Ga_{1/2}Sb_{1/2}O_6$ octahedra) characterized by a modulation wave-vector exactly perpendicular to [1,1,-2], for example, automatically creates rows of tetrahedra or octahedra along the same [1,1,-2] direction (see Fig.9a) that contain more or less of either the O' oxygen vacancies or of the Ga ions relative to the Sb ions.

The required expansion or contraction in size of the O'Bi_4 tetrahedra or $Ga_{1/2}Sb_{1/2}O_6$ octahedra that must necessarily accompany any such compositional modulation *i.e.* the displacive size effect relaxation (see *e.g.* Welberry, 1986, Butler *et al*, 1992 and Section III.D below) would therefore be different from one [1,1,-2] row of polyhedra to the next and hence would necessarily lead to macroscopic strain. As such, it does not occur (*i.e.* has zero amplitude, as shown experimentally by Fig.8).

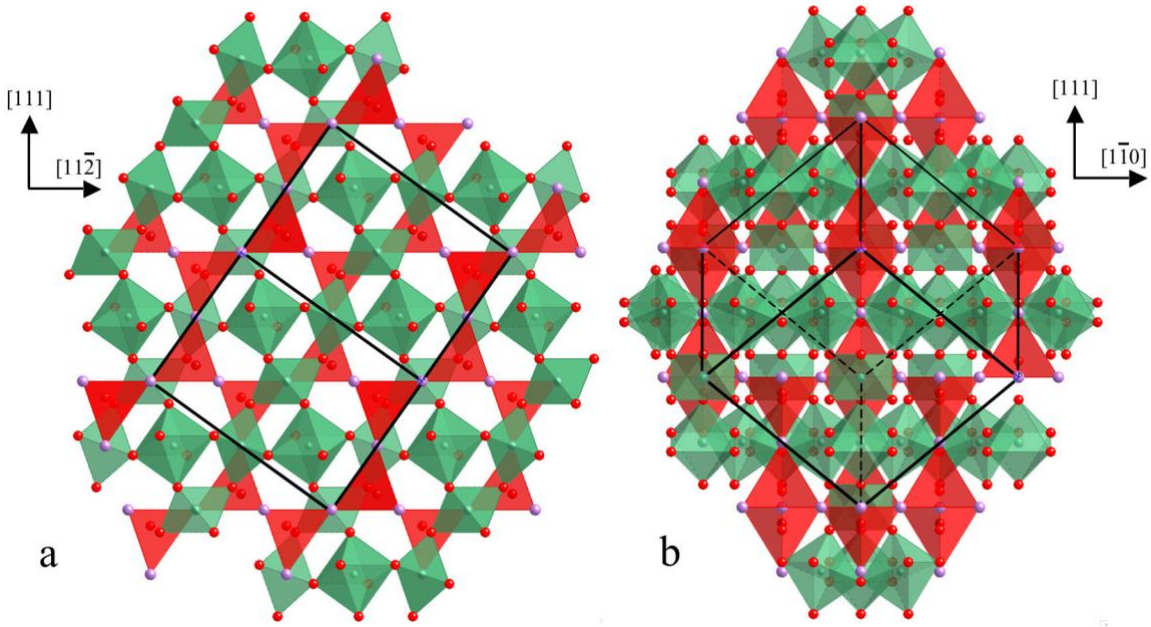

Fig.9 The disordered average structure of $Bi_{1.89}GaSbO_{6.84}$ - $(O'_{0.84}Bi_{1.89}).(GaSbO_6)$ is shown in projection down an (a) [1,-1,0] direction and (b) a [1,1,-2] direction. The [1,1,-2] direction is horizontal and the [111] direction vertical in (a) while the [1,-1,0] direction is horizontal and the [111] direction vertical in (b). The $O'_{0.84}Bi_{1.89}$ tetrahedral sub-structure, built out of O'Bi_4 tetrahedra, is shown in red and the $(GaSb)O_6$ octahedral sub-structure, built out of $Ga_{1/2}Sb_{1/2}O_6$ octahedra, in green. The average structure unit cell is outlined in each case.

The existence of "dark planes" in the midst of diffuse intensity distributions has only rarely been noticed let alone reported and hence the theoretical understanding of the phenomenon is not so well developed as other areas of diffuse scattering theory. Nonetheless, it is clear that the avoidance of macroscopic strain along high symmetry, closest contact directions of the atoms or constituent polyhedra of the underlying average structure plays a

very important role in the crystal chemistry underlying the existence of these planar diffuse absences (see *e.g.* Welberry, 1986, Butler *et al*, 1992).

III.D *Size Effect*

From the diffraction point of view, the size effect refers to the marked transferring of intensity from regions on one side of average structure Bragg reflections to the other. It is usually attributed to a mixed compositional and displacive contribution to the scattered intensity arising from the displacive relaxations accompanying compositional ordering (Warren *et al*, 1951, Borie and Sparks, 1971, Welberry, 1986, Welberry and Butler, 1994) and was first described in the context of disordered binary alloy phases (Warren *et al*, 1951).

The same effect is quite commonly observed in a range of other types of disordered phases. Fig.10c, for example, shows an <001> type zone axis EDP typical of the disordered Bi-based pyrochlore $(Bi_{1.5}Zn_{0.5})(Ti_{1.5}Nb_{0.5})O_7$ ~ $(O'Bi_{1.5}Zn_{0.5}).(Ti_{1.5}Nb_{0.5}O_6)$ (BZNT). In addition to the strong, sharp Bragg reflections of the underlying *Fd*-3*m*, pyrochlore type average structure, note the presence of characteristic 'blobs' of additional diffuse intensity (verging on additional satellite reflections) at the **G** ± <001>* regions of reciprocal space whose intensity is systematically stronger on the low angle side of the associated parent Bragg reflection than on the high angle sides (*cf. e.g.* the relative intensities of the 'satellite' reflections surrounding the [-8,8,0]* parent Bragg reflection encircled by the square white box in Fig.10c).

These **G** ± <001>* 'satellite' reflections arise from compositional Bi/Zn ordering on the $(O'Bi_{1.5}Zn_{0.5})$ tetrahedral sub-structure (see Fig.10a) of the pyrochlore average structure type (shown in a different context in Fig.9). As a result of local crystal chemical considerations (see Liu *et al*, 2006 for the details), the O' ions move out of the centre of each tetrahedra towards the Zn ions which in turn induces a coupled 'size effect' like relaxation of

the surrounding Bi and Zn ions (shown in Fig.10b). Without this 'size effect' like displacive relaxation (corresponding to a systematic expansion of the nearest neighbour [nn] Bi-Bi distances and a corresponding systematic reduction of the nn Bi-Zn distances) accompanying the Bi/Zn compositional ordering, the characteristic size effect induced transfer of intensity from the high to the low angle side of the neighbouring Bragg reflections is missing. With this displacive relaxation included, however, the observed intensity re-distribution is clearly quite well described (*cf. e.g.* the simulated [001] zone axis EDP of Fig.10d with the experimental one shown in Fig.10c; for more details see Liu *et al*, 2006).

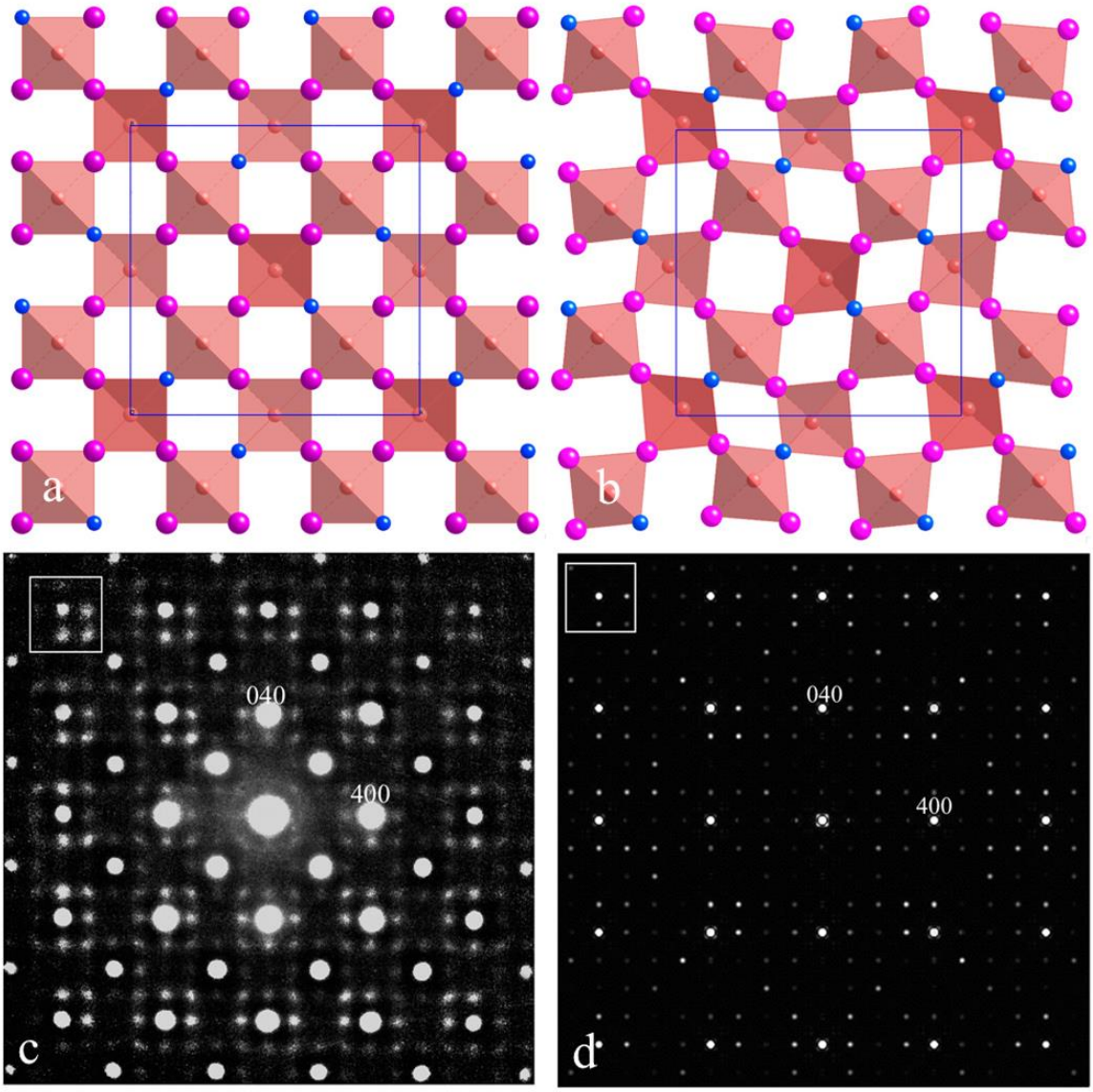

Fig.10 (a) The Bi/Zn ordered (O'$Bi_{1.5}Zn_{0.5}$) tetrahedral sub-structure of BZNT responsible for the **G** ± <001>* 'satellite' reflections apparent in the <001> zone axis EDP of BZNT shown in (c). The Bi

ions are represented by the large pink balls and the Zn ions by the smaller blue balls. The O' ions are in the centre of the O'Bi_3Zn tetrahedra in (a). (b) shows the size effect relaxed Bi/Zn distribution while (d) shows the simulated EDP corresponding to (b). For more details, see Liu *et al*, 2006.

III.E *The effects of multiple scattering and how to minimize them*

It should be clear from the above that a great deal of extremely useful information as to the nature of the structural disorder giving rise to structured diffuse distributions can be extracted via the use of the purely kinematic structure factor expression given in Eqn.(5) above. The possibility of multiple scattering obscuring this information when using electron diffraction, however, should never be ignored. While EDP's such as Fig.4a and Fig.5b demonstrate clearly that the theoretical possibility of multiple scattering involving more than one individual modulation wave-vector on the primary diffuse distribution can safely be ignored, the possibility/probability of a re-distribution of the kinematic primary diffuse distribution by strongly excited parent Bragg reflections usually can not. Fig.11, for example, shows an (a) close to [001], (b) [0,-1,3] and (c) [001] zone axis EDP's of the O/F disordered oxyfluoride FeOF.

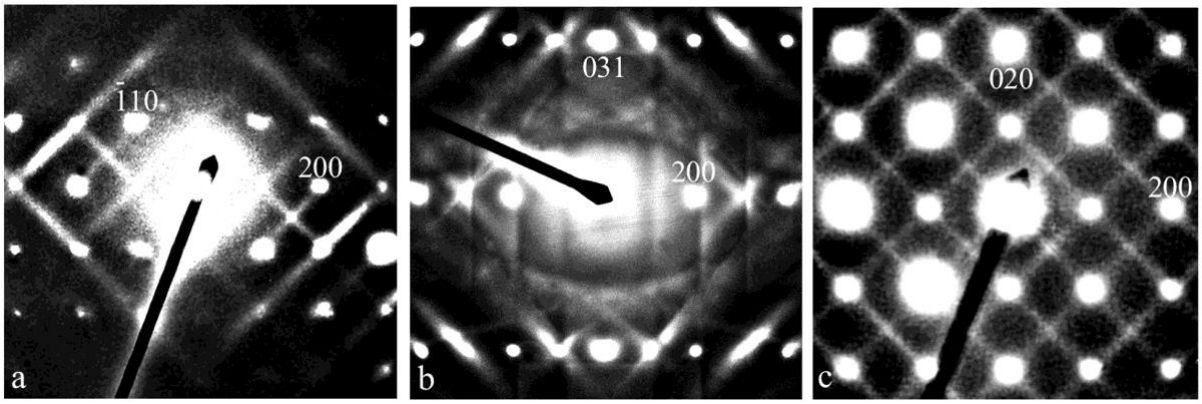

Fig.11 (a) close to [001], (b) [0,-1,3] and (c) [001] zone axis EDP's of the disordered oxyfluoride FeOF. For details, see Brink *et al*, 2000.

In the case of (a) and, in particular, (b) note the presence of a clear pseudo-extinction condition in that the observed diffuse only runs through the parent *hkl*, *h+k+l* odd reflections. In the case of (c), however, the observed diffuse runs through both *hkl*, *h+k+l* odd, as well as even, reflections. This is clearly due to a re-distribution of the rather more kinematic diffuse

intensity distribution apparent in Fig.11a by significantly more strongly excited *h+k+l* odd parent Bragg reflections at the exact zone axis orientation leading to an apparent break in the pseudo-extinction condition (for a real space description of the structural origin of the pseudo-extinction condition itself, see Brink *et al*, 2000, Withers, 2005). By tilting off axis somewhat (as in Fig.11a), this intensity re-distribution effect is significantly reduced and the kinematic pseudo-extinction condition again becomes apparent.

A most important way to avoid missing the existence of such pseudo-extinction conditions (and the critical insight they often provide into the structural distortions responsible, see *e.g.* Section III.B above) is to minimize the dynamical re-distribution of the kinematic diffuse intensity by deliberately taking EDP's a few degrees off-axis so as to keep the low order parent Bragg reflections causing the intensity re-distribution as weak as possible. An alternative method is to take EDP's at more minor zone axis orientations where the effect of multiple scattering from parent Bragg reflections can often be significantly reduced (*cf. e.g.* the [0,-1,3] zone axis EDP of FeOF shown in Fig.11b with the exact [001] zone axis EDP shown in Fig.11c). In practice, it is acknowledged that it is never possible to entirely remove the effects of multiple scattering by such means. Provided one is aware of the probability of intensity re-distribution via multiple scattering , however, it is usually possible to extract the desired information from experimental EDP's via application of one or other of the above approaches.

IV. SELECTED CASE STUDIES

IV.A *Compositionally 'disordered', NaCl-related, solid solution phases*

Many compositionally disordered solid solution phases that have a *NaCl*-type average structure (such as, for example, $LiFeO_2$ (Brunel *et al*, 1972), the widely sub-stoichiometric, transition metal carbide and nitride (MC_{1-x} and MN_{1-x}) solid solution phases (Billingham *et*

al, 1972, Brunel *et al*, 1972, Sauvage and Parthé, 1972) or the wide range non-stoichiometric $(1\text{-}x)M^{2+}S.xLn_{2x/3}{}^{3+}S$, *M* = Mg, Ca, Mn, *Ln* = a rare earth ion or Y, solid solution phases (Flahaut, 1979, Withers *et al*, 1994a, 2007)) exhibit a highly structured and characteristic diffuse intensity distribution accompanying the strong average structure Bragg reflections which is well-described by the relatively simple expression $\cos\pi h + \cos\pi k + \cos\pi l = 0$ (Billingham *et al*, 1972, Sauvage and Parthé, 1972, 1974, de Ridder *et al*, 1976a, b, 1977a, b Withers *et al*, 2003a, 2007).

Fig.12, for example, shows (a) <001>, (b) <110> and (c) <3,0,-1> zone axis EDP's typical of the 'disordered' $(1\text{-}x)Mg^{2+}S.xYb_{2x/3}{}^{3+}S$, $0 \leq x \leq 0.45$, solid solution phase for x = 0.30. Figs.12d, e and f show the equivalent calculated sections through the diffuse surface $\cos\pi h + \cos\pi k + \cos\pi l = 0$. Clearly there is very good agreement between the experimental EDP's and the calculated sections.

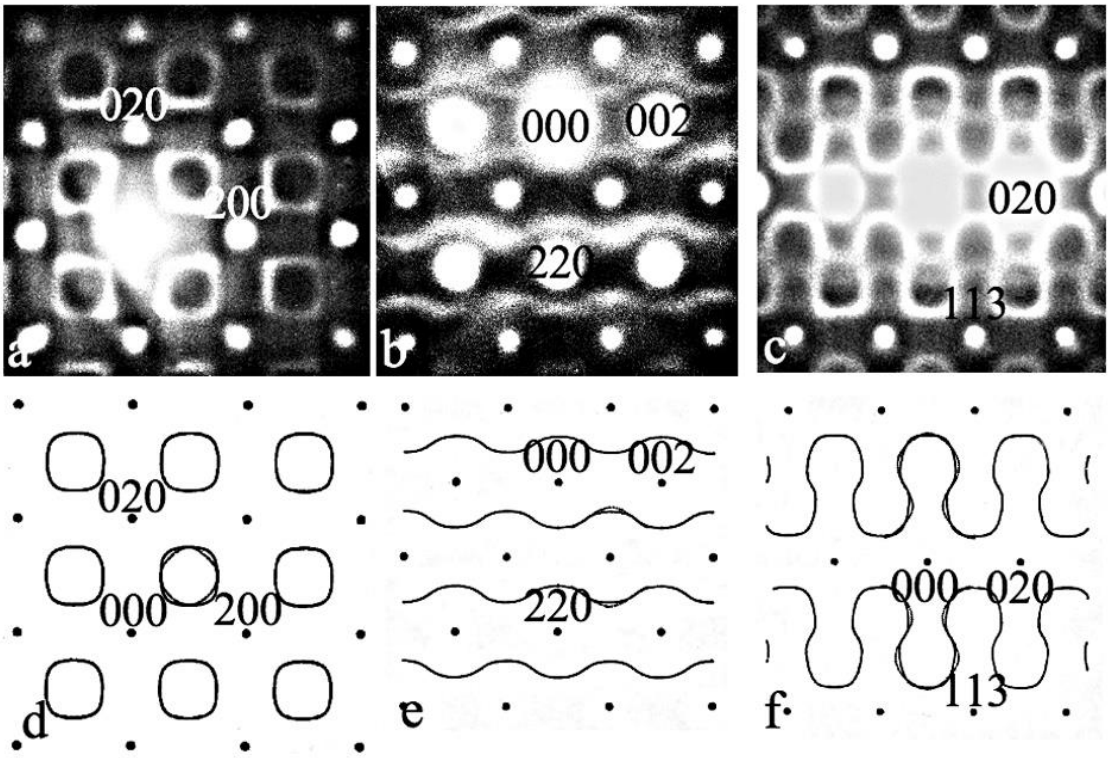

Fig.12. (a) <001>, (b) <110> and (c) <3,0,-1> zone axis EDP's typical of the 'disordered' $(1\text{-}x)Mg^{2+}S.xYb_{2x/3}{}^{3+}S$, $0 \leq x \leq 0.45$, solid solution phase for x = 0.30. (d), (e) and (f) show the

equivalent calculated sections through the diffuse surface $\cos\pi h + \cos\pi k + \cos\pi l = 0$ (taken from Sauvage and Parthe, 1972).

Why should this be so and what is the real space meaning of this reciprocal space relationship? Re-writing the expression $\cos\pi h + \cos\pi k + \cos\pi l = 0$ in the form

$\exp(2\pi i\mathbf{q}.{}^1/_2\,\mathbf{a})+\exp(-2\pi i\mathbf{q}.{}^1/_2\,\mathbf{a})+\exp(2\pi i\mathbf{q}.{}^1/_2\,\mathbf{b})+\exp(-2\pi i\mathbf{q}.{}^1/_2\,\mathbf{b})+\exp(2\pi i\mathbf{q}.{}^1/_2\,\mathbf{c})+\exp(-2\pi i\mathbf{q}.{}^1/_2\,\mathbf{c}) = 0$

(where $\mathbf{q} = h\mathbf{a}^*+k\mathbf{b}^*+l\mathbf{c}^*$, h, k and l continuous) suggests that a well-defined such shape in reciprocal space implies a well-defined and strongly obeyed multi-body correlation (see *e.g.* Welberry, 2004) in real space, in this case a six-body correlation involving a central atom and six surrounding atoms at $\pm{}^1/_2\,\mathbf{a}$, $\pm{}^1/_2\,\mathbf{b}$ and $\pm{}^1/_2\,\mathbf{c}$ with respect to the central atom.

In the specific case of $(1\text{-}x)Mg^{2+}S.xYb_{2x/3}{}^{3+}S$, x = 0.30, *i.e.* for $Mg_{0.7}Yb_{0.2}\square_{0.1}S$ (□ a vacancy) of defect *NaCl* average structure type, this real space correlation amounts to a requirement that each S ion (at position **t**) should be surrounded, as far as possible, by the average number of Mg^{2+} and Yb^{3+} ions (as well as □'s) in its nearest neighbour octahedral co-ordination polyhedron (see *e.g.* Sauvage and Parthé, 1972, 1974, Withers *et al*, 2007) *i.e* as far as possible there should always be 4.2 Mg ions, 1.2 Yb ions and 0.6 □'s vacancy in the nearest neighbour octahedron of surrounding *M* ions (at $\mathbf{t}\pm{}^1/_2\mathbf{a}$, $\mathbf{t}\pm{}^1/_2\mathbf{b}$ and $\mathbf{t}\pm{}^1/_2\mathbf{c}$).

In the language of the modulation wave approach

$$\delta f_M(\mathbf{t}+{}^1/_2\mathbf{a})+\delta f_M(\mathbf{t}-{}^1/_2\mathbf{a})+\delta f_M(\mathbf{t}+{}^1/_2\mathbf{b})+\delta f_M(\mathbf{t}-{}^1/_2\mathbf{b})+\delta f_M(\mathbf{t}+{}^1/_2\mathbf{c})+\delta f_M(\mathbf{t}-{}^1/_2\mathbf{c})$$
$$= 2f_M{}^{av}\,\Sigma_{\mathbf{q}}\,a_M(\mathbf{q})\,\exp 2\pi i\mathbf{q}.\mathbf{t}\,\{\cos 2\pi\mathbf{q}.{}^1/_2\mathbf{a}+\cos 2\pi\mathbf{q}.{}^1/_2\mathbf{b}+\cos 2\pi\mathbf{q}.{}^1/_2\mathbf{c}\}$$

should always equal zero regardless of the value of **t**. The only way this can be true for all **t** is if $\{\cos 2\pi\mathbf{q}.{}^1/_2\,\mathbf{a}+\cos 2\pi\mathbf{q}.{}^1/_2\,\mathbf{b}+\cos 2\pi\mathbf{q}.{}^1/_2\,\mathbf{c}\} = \cos\pi h + \cos\pi k + \cos\pi l = 0$, just as is observed experimentally. Of course, at the local level it is not possible to have 4.2 Mg ions, 1.2 Yb ions and 0.6 □'s vacancies surrounding each S ion. What the constraint implies is that the local octahedral configurations closest in composition to this, *i.e.* $Mg_4Yb_1\square_1$, $Mg_5Yb_1\square_0$, and $Mg_4Yb_2\square_0$, must be heavily favoured and occur most most commonly. Note that the

overall macroscopic stoichiometry results if only these three local configurations ever occur and if the relative proportions of their occurrence are 60 %, 20 % and 20 % respectively (see Withers *et al*, 2007 for further details).

The observed diffuse distribution is thus the characteristic signature in reciprocal space of the real space condition that the smallest polyhedral building blocks of the average *NaCl* structure type (the SM_6 octahedra) should each have, as far as possible, the same composition as the overall macroscopic composition ($SMg_{4.2}Yb_{1.2}\square_{0.6}$) in order to minimize substitutional strain. Such a local occupational ordering constraint is entirely reasonable from the local crystal chemical point of view (see Withers *et al*, 2007). It is also the basis of the so-called cluster expansion approach to compositionally disordered solid solution phases based originally upon an idea of Pauling (1960) and subsequently expanded upon, developed and successfully applied by Brunel *et al* (1972), Sauvage and Parthé (1972, 1974) and de Ridder *et al* (1976a,b, 1977a,b) to a range of substitutional order/disorder problems.

The same approach has also been successfully applied to a range of other local polyhedral cluster shapes including *e.g* tetrahedra, cubes, trigonal prisms *etc.* In each case case, different diffuse intensity surfaces have been predicted (see *e.g* Sauvage and Parthé, 1974, de Ridder *et al*, 1976a, b, Liu *et al*, 2006) and, in many cases, verified experimentally.

IV.B *Inherently flexible, tetrahedrally corner-connected framework structures*

Inherently flexible, tetrahedrally corner-connected framework structures such as *e.g.* the quartz, cristobalite and tridymite forms of silica, SiO_2, and $AlPO_4$ or many of the members of the large family of microporous zeolitic aluminosilicate and zeotypic aluminophosphates, particularly those exhibiting apparent 180° *T*-O-*T* (*T* = Al, Si, P *etc.*) angles (see *e.g.* Fig.13) represent another broad class of (displacively) disordered materials which often exhibit highly structured diffuse intensity distributions.

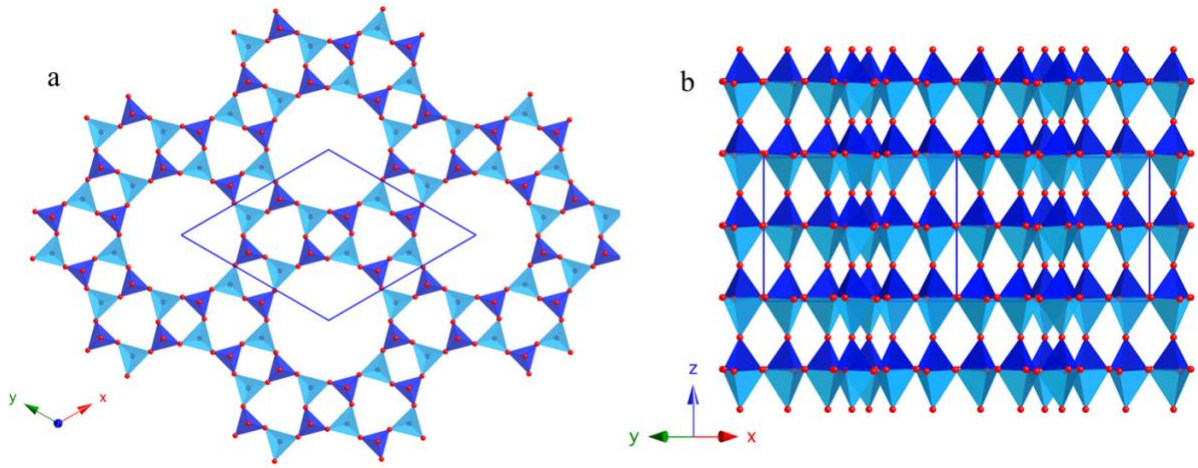

Fig.13. An (a) [001] and (b) [110] projection of the disordered average crystal structure of the microporous aluminophosphate, $AlPO_4$-5. The larger AlO_4 tetrahedra are light blue and the smaller PO_4 tetrahedra dark blue in (b). The unit cell is shown in outline in both (a) and (b). Note the existence of apparent 180° Al-O-P angles along the *c* direction in (b).

Despite the inherent rigidity of the tetrahedral building blocks of these materials, they are often strongly polymorphic (see *e.g.* Pryde and Dove, 1998) and, in their high temperature, high symmetry polymorphic forms, usually dynamically disordered as a result of the simultaneous excitation of numerous, essentially zero frequency, Rigid Unit Mode (RUM) modes of distortion (Dove *et al*, 1998, 2002) involving changes in the relative orientation of neighbouring polyhedral units without distorting either the shape or size of the individual polyhedral units themselves (see *e.g.* Fig.14).

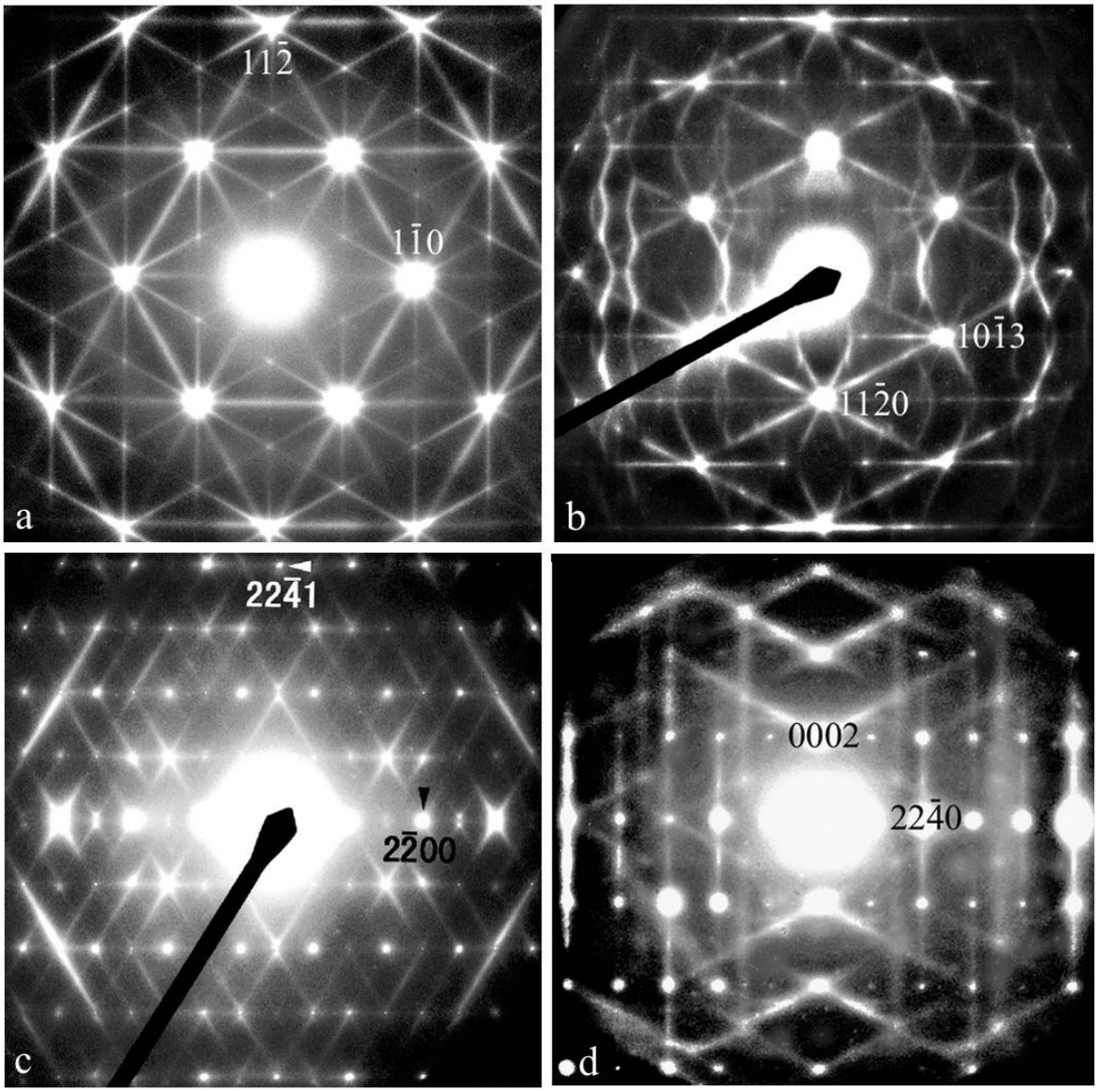

Fig.14. (a) <111>, (b) <-3,3,1>, (c) <1,1,-4> and (d) [-1,1,0] zone axis EDP's typical of (a) the β-cristobalite form of SiO_2 above 270 °C, (b) SiO_2-tridymite above 250 °C, (c) β-hexacelsian above 310 °C and (d) room temperature $AlPO_4$-5.

The sharp, continuous diffuse intensity distributions observed in EDP's from materials of this type (see *e.g.* Fig.14) map out the zero energy cost, or 'zero frequency', Rigid Unit Mode (RUM) phonon modes of distortion of these various inherently flexible framework structures.

For these materials, the relevant constraint giving rise to the observed structured diffuse distribution is not this time a local compositional constraint but rather a requirement that the individual polyhedral units should not be distorted by the particular soft phonon mode involved. As the oxygen ions in such framework structures typically link together two

such tetrahedral units (see *e.g.* Fig.13), it is clear that the only allowable soft modes will be those involving necessarily coupled correlated tetrahedral rotations and translations of neighbouring, essentially rigid, tetrahedral units. The topological connectivity of the individual tetrahedral units involved is thus crucial in determining the allowed modulation wave-vectors and hence the observed diffuse distribution.

The topological connectivity of the constituent SiO_4 tetrahedral units in the case of the β-cristobalite form of SiO_2, for example, gives rise to soft phonon modes with modulation wave-vectors localized to reciprocal lattice directions perpendicular to the six <110> directions of real space (see *e.g* Fig.13a, see also Withers, 2005). In other cases, however, the shape of the observed diffuse distribution is considerably more complex (see *e.g.* Fig.13b). In the case of the tridymite form of SiO_2, for example, the topological connectivity of the constituent SiO_4 tetrahedral units gives rise to a curved diffuse distribution intensity distribution whose analytical shape is well-described by the expression $\sin^2\pi l = {}^8/_9\{1-\cos\pi h \cos\pi k \cos\pi(h+k)\}$ (see Withers, 2003b for the details).

Whatever the particular details involved in any one particular case, it is the topological connectivity of the tetrahedral units involved that always determines the allowed patterns of correlated polyhedral rotations and translations and hence the shapes of the resultant observed diffuse distributions. Such materials are fundamentally "jelly-like" and unavoidably displacively disordered. A proper understanding of the local crystal chemistry as well as of the fundamental physico-chemical properties of such materials requires an understanding of this inherent coupled orientational and translational flexibility.

IV.C *The non-magnetic Kondo effect material ThAsSe and the role of the Fermi surface*

Low dimensional materials susceptible to Charge Density Wave (CDW) type structural instabilities, such as the non-magnetic Kondo effect material ThAsSe, also often

exhibit highly structured diffuse intensity distributions which effectively map out the Fermi surface of the undistorted parent structure. Fig.15a, for example, shows an [001] zone axis EDP of ThAsSe taken at 100 K while Fig.15c shows the clearly closely related, calculated Fermi Surface (FS) of ThAsSe in projection along *c**.

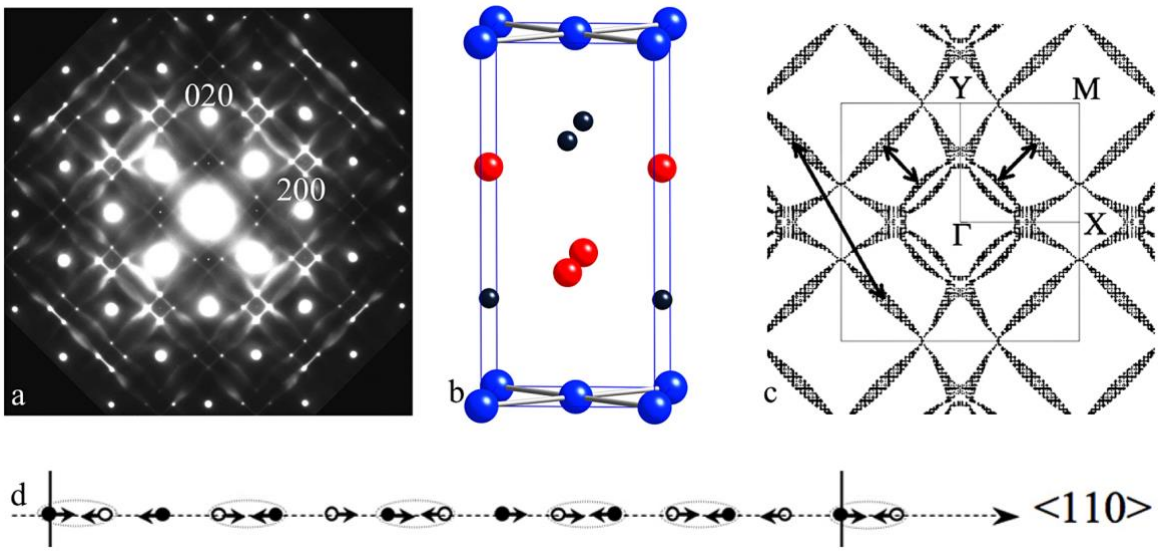

Fig.15. (a) An [001] zone axis EDP of ThAsSe taken at 100 K, (b) the *P*4/*nmm* average structure of ThAsSe (As ions represented by the large blue balls, Se ions by the medium sized red balls and Th ions by the small black balls) and (c) the calculated Fermi Surface (FS) of ThAsSe in projection along *c**. Some **q**-vectors spanning this FS are marked on (c). (d) shows the pattern of As-As dimerization responsible for the observed diffuse distribution (see Withers *et al*, 2006 for details).

Additional EDP's taken on tilting away from this [001] zone axis orientation (see Withers *et al*, 2004, 2006 for details) show that the diffuse 'streaking' in Fig.15a is, in fact, part of sheets of **G** ± ~0.14 <110>* ± ε <1,-1,0>* + η [001]* (ε and η continuous) diffuse intensity running perpendicular to the two <110> directions of real space. The *P*4/*nmm* average structure of ThAsSe is shown in Fig.15b while the calculated Fermi Surface (FS) of the undistorted ThAsSe parent structure in projection along *c** is shown in Fig.15c.

Temperature-dependent electron diffraction shows that the highly structured diffuse intensity distribution characteristic of ThAsSe at low temperature is the result of the gradual condensation of a 1-d CDW and associated pattern of As-As dimerization (shown in Fig.15d), correlated in 1-d strings along <110> directions but not correlated from one <110>

string to the next. Electronic band structure calculations (see Withers *et al*, 2006) show that the ~ 7 times periodicity of this As-As dimerization along each of the two <110> real space directions is determined by the FS of the undistorted parent structure. The **q**-vectors, obtained by measuring the distances between the flattened parts of the corresponding FS are in remarkably good accord with the values determined from the electron diffraction patterns (*cf. e.g.* Fig.15c with Fig.15a).

IV.D *Materials susceptible to ferroelastic strain distortions such as α-PbO*

The *P*4/*nmm*, layered, tetragonal α form of PbO (a_t = 3.9719, c_t = 5.023Å, subscript t for tetragonal parent structure, at room temperature, see Fig.16 below) undergoes a low temperature, incommensurate phase transition in the vicinity of 208 K.

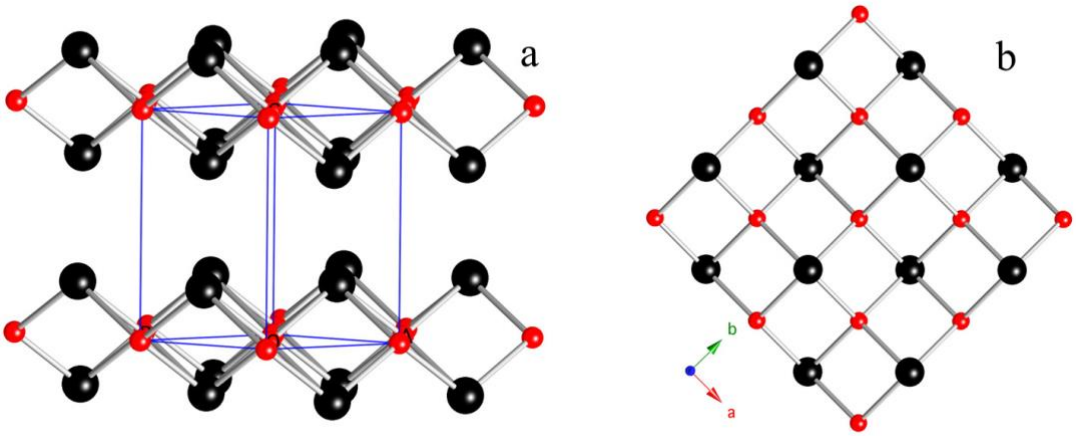

Fig.16. (a) A close to <110> and (b) [001] projection of the *P*4/*nmm*, tetragonal α form of PbO. The small red balls represent the O ions and the larger dark balls the Pb ions. Note that the O ions form square arrays in (001) planes and that each oxygen ion is tetrahedrally co-ordinated by Pb ions.

It was first noticed because it is improper ferroelastic (Boher *et al*, 1985; Moreau *et al*, 1989; Withers *et al*, 1993, Withers and Schmid, 1994) *i.e.* the freezing out of an incommensurate **q** ~ 0.185(-$\mathbf{a}_t$*+$\mathbf{b}_t$*) displacive modulation on cooling below ~208 K induces an orthorhombic strain distortion of the underlying tetragonal sub-structure leading to a *Cmma* (**a** = $\mathbf{a}_t$ + $\mathbf{b}_t$, **b** = -$\mathbf{a}_t$ + $\mathbf{b}_t$, **c** = $\mathbf{c}_t$) average structure for the low temperature phase.

Moreau *et al.* (1989) reported the existence of a significant precursor diffuse background in neutron powder diffraction profiles of α-PbO at room temperature above this low temperature transition but were unable to determine the distribution in reciprocal space of this diffuse distribution. Room temperature [001] zone axis EDP's show the presence of extremely characteristic diffuse crosses centred on each Bragg reflection and running along the $<110>_t$* directions of reciprocal space (see *e.g.* Fig.17a). EDP's taken on tilting away from [001] (see *e.g.* the [0,-1,2] zone axis EDP shown in Fig.17b) show that the diffuse distribution is not confined to the <110>* directions of reciprocal space but rather takes the form of quite narrow discs or ellipses of diffuse intensity perpendicular to the $<110>_t$ directions of real space *i.e.* the diffuse always runs along the <*hhl*>* directions of reciprocal space *e.g.* along the [221]* and [-2,2,1]* directions of reciprocal space in Figs.17b. Note also that the corresponding real space displacive modulations responsible are necessarily transverse polarized as shown by the <-1,1,0>* systematic row EDP shown in Fig.17d (see also Section III.A above).

This type of characteristic diffuse distribution is strongly reminiscent of the diffuse streaking present in many materials susceptible to a change in crystal class at a phase transformation such as *e.g.* the partially ordered potassium feldspars (McClaren and Fitz Gerald, 1987), doped 1:2:3 oxide superconductors (Schmahl *et al*, 1989) and disordered seminconductor alloy phases (see *e.g.* Treacy *et al*, 1985). Its presence demonstrates that the room temperature *P*4/*nmm* structure of α-PbO shown in Figure 16 is only a time and space averaged structure. Diffraction contrast images of these types of materials typically show a characteristic "tweed" microstructure. A rather similar tweed microstructure (exhibiting a minimum dimension of ~ 20 Å) can also be observed in α-PbO, as shown in the ~ [001] zone axis room temperature DF micrograph of Fig.17c.

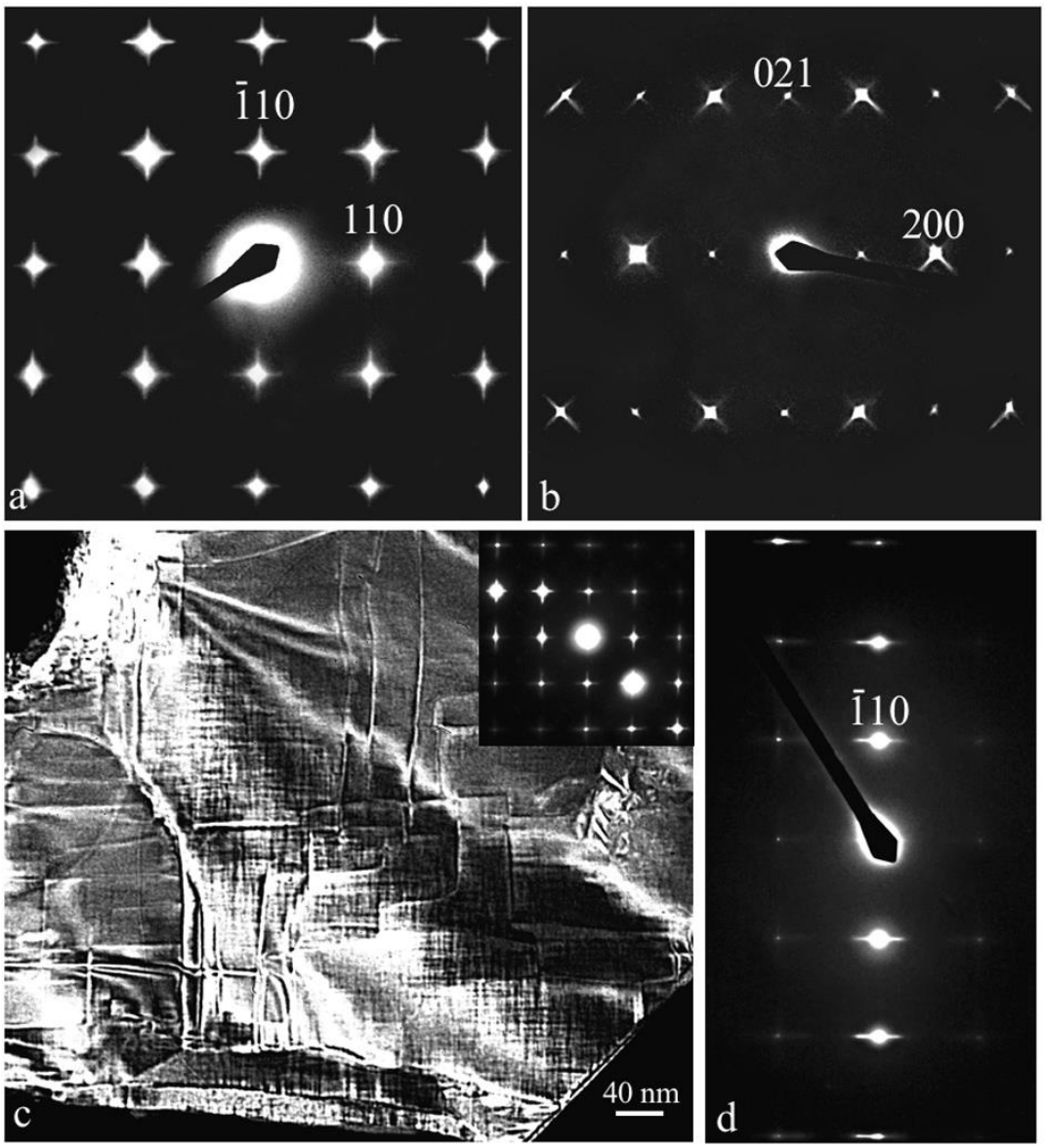

Fig.17. Room temperature (a) [001] and (b) [0,-1,2] zone axis EDP's of α-PbO. (d) shows a [-1,1,0]* systematic row EDP and (c) a $[200]_t$* Dark Field (DF) image of α-PbO taken close to an [001] zone axis orientation. The corresponding EDP is inset. Note the characteristic tweed microstructure visible in the vicinity of the $[200]_t$* extinction bend contour. For details, see Withers *et al*, 1993.

Intriguingly, this tweed microstructure displayed dynamical behaviour in that bands of tweed contrast changed in appearance ("twinkled") in time scales of less than a second *i.e.* there is still some dynamical character to the instability at room temperature. In general, the narrowest bands of the tweed pattern changed contrast most rapidly so that images recorded typically over times of 5-10 seconds were dominated by the most stable and broad bands (see Withers *et al*, 1993 for more details).

The structural origin of the diffuse crosses and the corresponding tweed microstructure arise from the the instability of the α-PbO framework to long wavelength transverse shear waves characterized by modulation wave-vectors perpendicular to the two $<110>_t$ directions of real space (in much the same manner as the transverse modulated square atom array shown in Fig.6a). It would therefore appear that the room temperature *P*4/*nmm* structure of α-PbO resembles a 2-dimensional "jelly" in that it is unstable against specific long wavelength transverse shear waves. Indeed, on cooling below 208 K, one of these unstable transverse shear waves characterized by the incommensurate primary modulation wave-vector $\mathbf{q} \sim 0.185(-\mathbf{a}_t^*+\mathbf{b}_t^*)$ freezes out completely giving rise to the low temperature improper ferroelastic phase of α-PbO (see *e.g.* Withers and Schmid, 1994).

V. CONCLUSIONS

It is very much hoped that this review has demonstrated that there still remains a wealth of unexplained diffraction phenomena as well as detailed structural information to be extracted from careful electron diffraction investigations of 'disordered'/locally ordered materials and that the modulation wave approach to the description and interpretation of structured diffuse scattering is a particularly useful approach for this endeavour. The existence of absolute extinction conditions and pseudo-extinction conditions in diffuse distributions as well as the existence of 'dark planes' in diffuse distributions are important diffraction phenomena that deserve to be much more systematically exploited in investigations of 'disordered' materials.

Acknowledgements. The author acknowledges his debt of gratitude to many colleagues. In particular, thanks are due to his close colleague Richard Welberry. Thanks are also due to G. van Tendeloo, F.Brink, L.Norén, Y.Liu, R.Vincent, J.D.Fitz Gerald, S.Schmid, J.G.Thompson, J.M.Pérez-Mato, J.Etheridge and P.Midgeley for their interest in this area and

to F.Brink, I.R.Fisher and P.Midgeley for permission to reproduce material from joint publications. RLW acknowledges the Australian Research Council (ARC) for financial support in the form of ARC Discovery Grants. RLW would like to thank Peter Hawkes in particular for inviting him to write this review.

References

Anderson, J.S. (1984). Nonstoichiometric compounds: A critique of current structural views. *Proc. Indian Acad. Sciences (Chem. Sciences)* **93**, 861-904.

Andersson, S., Hyde, S.T. and Bovin, J-O. (1985). On the periodic minimal surfaces and the conductivity mechanism of α-AgI. *Z. für Kristallogr.* **173**, 97-99.

Andersson, S., Hyde, S.T., Larsson, K. and Lidin, S. (1988). Minimal surfaces and structures: from inorganic and metal crystals to cell membranes and biopolymers. *Chem. Reviews* **88**, 221-242.

Aragón, J.L, Terrones, H. and Romeu, D. (1993). Model for icosahedral aperiodic graphite structures. *Phys. Rev. B* **48**, 8409-8411.

Aroyo, M.I., Boysen, H. and Pérez-Mato, J.M. (2002a). Inelastic neutron scattering selection rules for phonons: application to leucite phase transitions. *Appl. Phys. A (Suppl.)* **74**, 1043-1045.

Aroyo, M.I., Boysen, H. and Pérez-Mato, J.M. (2002b). Application of phonon extinction rules in thermal diffuse scattering experiments. *Physica B* **316-317**, 154-157.

Billingham, J., Bell, P.S. and Lewis, M.H. (1972). Vacancy short-range order in substoichiometric transition metal carbides and nitrides with the NaCl structure. I. Electron diffraction studies of short-range ordered compounds. *Acta Cryst. A* **28**, 602-606.

Bindi, L., Evain, M. and Menchetti, S. (2006). Temperature dependence of the silver distribution in the crystal structure of natural pearceite, $(Ag,Cu)_{16}(As,Sb)_2S_{11}$. *Acta Cryst. B* **62**, 212-219.

Boher, P., Garnier, P., Gavarri, J.R. and Hewat, A.W. (1985). Monoxyde quadratique PbOα(I): Description de la transition structurale ferroélastique. *Journal of Solid State Chem.* **57**, 343- 350, 1985.

Borie, B. and Sparks, C.J. (1971). The interpretation of intensity distributions from disordered binary alloys. *Acta Cryst. A* **27**, 198-201.

Bradley, C.J. and Cracknell, A.P. (1972). *The Mathematical Theory of Symmetry in Solids*. Clarendon Press, Oxford.

Brink, F.J., Norén, L. and Withers, R.L. (2004). Electron diffraction evidence for continuously variable, composition-dependent O/F ordering in the ReO_3 type, $Nb^{V}_{1-x}Nb^{IV}_{x}O_{2-x}F_{1+x}$, $0 \leq x \leq 0.48$, solid solution. *Journal of Solid State Chem.* **177**, 2177-2182.

Brink, F.J., Withers, R.L. and Norén, L. (2002). An electron diffraction and crystal chemical investigation of oxygen/fluorine ordering in niobium oxyfluoride, NbO_2F. *Journal of Solid State Chem.* **166**, 73-80.

Brink, F.J., Withers, R.L. and Thompson, J.G. (2000) An electron diffraction and crystal chemical investigation of oxygen/fluorine ordering in rutile-type iron oxyfluoride, FeOF. *Journal of Solid State Chem.* **155**, 359-365.

Brunel, M., de Bergevin, F. and Gondrand, M. (1972). Determination theorique et domaines d'existence des differentes surstructures dans les composes $A^{3+}B^{1+}X_2^{2-}$ de type NaCl. *J. Phys. Chem. Sol.* **33**, 1927-1941.

Butler, B.D., Withers, R.L. and Welberry, T.R. (1992). Diffuse absences due to the atomic size effect. *Acta Cryst. A* **48**, 737-746.

Castles, J.R., Cowley, J.M. and Spargo, A.E.C (1971). Short-range ordering of vacancies and Fermi surface of TiO. *Acta Cryst. A* **27**, 376-383.

Comes, R., Lambert, M. and Guinier, A. (1968). The chain structure of $BaTiO_3$ and $KNbO_3$. *Solid State Commun.* **6**, 715-719

Dove, M.T., Heine, V. Hammonds, K.D., Gambhir, M. and Pryde, A.K.A. (1998). Short range disorder and long range order: implications of the Rigid Unit Mode model: In: *Local Structure from Diffraction* (Eds. S.J.L.Billinge and M.F.Thorpe), Plenum Press, New York, 253-271.

Dove, M.T., Tucker, M.G. and Keen, D.A. (2002) Neutron total scattering method: simultaneous determination of long-range and short range order in disordered materials. *Eur. J. Mineral.* **14**, 331-348.

Esmaeilzadeh, S., Lundgren, S., Halenius, U. and Grins, J (2001). $Bi_{1-x}Cr_xO_{1.5+1.5x}$, $0.05<x<0.15$: A new high temperature solid solution with a three-dimensional incommensurate modulation. *Journal of Solid State Chem.* **156**, 168-180.

Fisher, I.R., Kramer, M.J., Islam, Z., Wiener, T.A., Kracher, A., Ross, A.R., Lograsso, T.A., Goldman, A.I. and Canfield, P.C. (2000). Growth of large single-grain quasicrystals from high-temperature metallic solutions. *Materials Sci. and Engineering A* **294-296**, 10-16.

Flahaut, J (1979). in *Handbook on the Physics and Chemistry of the Rare Earths*, Eds. K.L.Gschneider and L.Eyring, North Holland, Amsterdam, Vol.4, Chapter 31, 1-88.

de Fontaine, D. (1972). An analysis of clustering and ordering in multicomponent solid solutions - I. Stability criteria. *J. Phys. Chem. Sol.* **33**, 297-310.

Funke, K. and Banhatti, R.D. (2006). Ionic motion in materials with disordered structures. *Solid State Ionics* **177**, 1551-1557.

Glazer, A.M (1972). The classification of tilted octahedra in perovskites. *Acta Crystallogr. B* **28**, 3384-3392.

Gomyo, A., Suzuki, T and Iijima, S. (1988). Observation of strong order in $Ga_xIn_{1-x}P$ alloy semiconductors. *Phys. Rev. Letts.* **60**, 2645-2648.

Harada, J. and Honjo, G. (1967). X-ray studies of the lattice vibration in tetragonal barium titanate. *J. Phys. Soc. Jpn.* **22**, 45-57.

Harburn, G., Taylor, C.A. and Welberry, T.R. (1975). *Atlas of Optical Transforms*, G.Bell and Sons Ltd., London.

Hartmann, V.M and Kevan, L (1999). Transition-Metal Ions in Aluminophosphate and Silicoaluminophosphate Molecular Sieves: Location, Interaction with Adsorbates and Catalytic Properties. *Chem. Rev.* **99**, 635-663.

Honjo, G., Kodera, S. and Kitamura, N (1964). Diffuse streak patterns from single crystals I. General discussion and aspects of electron diffraction diffuse streak patterns. *J. Phys. Soc. Japan* **19**, 351-367.

Iijima, S. (1991). Helical microtubules of graphitic carbon. *Nature* **354**, 56-58.

Ismunundar, Kennedy, B.J. and Hunter, B.A. (1999). Observations on pyrochlore oxide structures. *Mat. Res. Bull.* **34**, 1263-1274.

Jacob, M. and Andersson, S. (1998). *The nature of mathematics and the mathematics of nature.* Elsevier Press, Amsterdam.

Janner, A. (1997). De Nive Sexangula Stellata. *Acta Cryst. A* **53**, 615-631.

Janner, A. (2001). DNA enclosing forms from scaled growth forms of snow crystals. *Cryst. Engineering* **4**, 119-129.

Janssen, T., Chapuis, G. and de Boissieu, M. (2007). *Aperiodic Crystals from modulated phases to quasicrystals*. IUCr Monographs on Crystallography 20, Oxford University Press, Oxford.

Janssen, T., Janner, A., Looijenga-Vos, A. and de Wolff, P.M (1995). Incommensurate and commensurate modulated structures. In: Wilson AJC, ed. *International Tables for Crystallography*, Vol C. Dordrecht: Kluwer Academic Publishers, 797-835.

Khanna, S.K., Pouget, J.P., Comes, R., Garito, A.F. and Heeger, A.J. (1977). X-ray studies of $2k_F$ and $4k_F$ instabilities in tetrathiafulvalene-tetracyanoquinodimethane (TTF-TCNQ). *Phys. Rev. B* **16**, 1468-1479.

Klinowski, J., Mackay, A.L. and Terrones, H. (1996). Curved surfaces in Chemical Structure. *Phil. Trans. Roy. Soc. Lond.* A **354**, 1975-1987.

Krivoglaz, M.A. (1969). *The theory of X-ray and thermal neutron scattering by real crystals.* Plenum Press, New York.

Kroto, H.W., Heath, J.R., O'Brien, S.C., Curl, R.F. and Smalley, R.E. (1985). C_{60}: buckminsterfullerence. *Nature* **318**, 162-163.

Liu, Y., Withers, R.L., Nguyen, B. and Elliott, K. (2007). Structurally frustrated polar nanoregions in $BaTiO_3$-based relaxor ferrolectric systems. *Appl. Phys. Letts.* **91**, 152907.

Liu, Y., Withers, R.L. and Norén, L (2003). An electron diffraction, XRD and lattice dynamical investigation of the average structure and RUM modes of distortion of microporous $AlPO_4$-5. *Solid State Sciences* **5**, 427-434.

Liu, Y., Withers, R.L. and Wei, XY (2005). Structurally frustrated relaxor ferroelectric behaviour in $CaCu_3Ti_4O_{12}$. *Phys. Rev. B* **72**, 134104:1-4.

Liu, Y., Withers, R.L., Welberry, T.R., Wang, H. and Du, H. (2006). Crystal chemistry on a lattice: The case of BZN and BZN-related pyrochlores. *Journal of Solid State Chem.* **179**, 2141-2149.

Mackay, A.L. (1976). Crystal symmetry. *Physics Bulletin* (November Edition) 495-497.

Mackay, A.L. (1981). De Nive Quinquangula. On the pentagonal snowflake. *Sov. Phys. Crystallogr.* **26**, 517-522.

Mackay, A.L. (1988). New geometries for superconduction and other purposes. *Speculations in Science and Technology* **11**, 4-8.

Matsumura, S., Takano, K., Kuwano, N. and Oki, K (1991). Dynamical Monte Carlo simulation of $L1_1$ (CuPt)-type ordering during (001) epitaxial growth of III-V semiconductor alloys. *J. of Crystal Growth* **115**, 194-198.

McLaren, A.C. and Fitz Gerald, J.D. (1987). CBED and ALCHEMI investigations of local symmetry and Al,Si ordering in K-feldspars. *Phys. Chem. Min.* **14**, 281-292.

Moreau, J., Kiat, J.M., Garnier, P. and Calvarin, G. (1989). Incommensurate phase in lead monoxide α- PbO below 208K. *Phys. Rev. B* **39**, 10296-10299.

Moreno, M.S., Varela, A. and Otero-Diaz, L.C. (1997). Cation non-stoichiometry in tin-monoxide-phase $Sn_{1-\delta}$ with tweed microstructure. *Phys. Rev. B* **56**, 5186-5192.

Moret, R., Huber, M. and Comes, R (1977). Short-range and long-range order of titanium in titanium sulfide ($Ti_{1+x}S_2$). *Journal de Physique, Colloque* **7**, 202-206.

Norman, P.D., Morton, A.J., Wilkins, S.W. and Finlayson, T.R (1985). Imaging the Fermi surface of β'-brass through electron diffuse scattering. *Metals Forum* **8**, 43-48.

Ohsima, K. and Watanabe, D (1973). Electron diffraction study of short-range-order diffuse scattering from disordered Cu-Pd and Cu-Pt alloys. *Acta Cryst. A* **29,** 520-526.

Otero-Diaz, L.C., Withers, R.L., Gomez-Herrero, A., Welberry, T.R. and Schmid, S. (1995). A TEM and XRD study of $(BiS)_{1+\delta}(Nb_{1+\varepsilon}S_2)_n$ misfit layer structures. *Journal of Solid State Chem.* **115**, 274-282.

Pauling, L. (1985). Apparent icosahedral symmetry is due to directed multiple twinning of cubic crystals. *Nature* **317**, 512-514.

Pérez-Mato, J.M., Madariaga, G. and Tello, M.J. (1986). Diffraction symmetry of incommensurate structures. *J. Phys. C: Solid State Phys.* **19**, 2613-2622.

Pérez-Mato, J.M., Madariaga, G., Zuniga, F.J. and Garcia Arribas, A. (1987). On the structure and symmetry of incommensurate phases. A practical formulation. *Acta Cryst. A* **43**, 216-226.

Pérez-Mato, J.M., Aroyo, M., Hlinka, J., Quilichini, M. and Currat, R. (1998). Phonon symmetry selection rules for inelastic neutron scattering. *Phys. Rev. Letts.* **81,** 2462-2465.

Petricek,V., Dusek, M. and Palatinus, L. (2000). *Jana2000. The crystallographic computing system*. Institute of Physics, Praha, Czech Republic.

Pryde, A.A. and Dove, M.T. (1998). On the sequence of phase transitions in tridymite. *Phys. Chem. Min.* **26**, 171-179.

Putnis, A. and Salje, E. (1994). Tweed microstructures: experimental observations and some theoretical models. *Phase Transitions* **48**, 85-105.

de Ridder, R., van Dyck, D., van Tendeloo, G. and Amelinckx, S (1977a). A cluster model for the transition state and its study by means of electron diffraction II. Application to some particular systems. *Phys. Stat. Sol.* (a) **40**, 669-683.

de Ridder, R., van Tendeloo, G. and Amelinckx, S (1976a). A cluster model for the transition from the short range order to the long range order state in f.c.c based binary systems and its study by means of electron diffraction. *Acta Cryst. A* **32**, 216-224.

de Ridder, R., van Tendeloo, G., van Dyck, D. and Amelinckx, S (1976b). A cluster model for the transition state and its study by means of electron diffraction I. Theoretical model. *Phys. Stat. Sol. (a)* **38**, 663-674.

de Ridder, R.. van Tendeloo, G., van Dyck, D. and Amelinckx, S. (1997b). The transition state as an interpretation of diffuse intensity contours in substitutionally disordered systems. *J. de Physique Colloque C7* **38**, 178-186.

Sato, H., Watanabe, D. and Ogawa, S. (1962). Electron diffraction study on CuAu at temperatures above the transition point of order-disorder. *J. Phys. Soc. Japan* **17**, 1647-1651.

Sauvage, M. and Parthé, E. (1972). Vacancy short range order in substoichiometric transition metal carbides and nitrides with the NaCl structure. II. Numerical calculation of vacancy arrangement. *Acta Cryst. A* **28**, 607-616.

Sauvage, M. & Parthé, E. (1974). Prediction of diffuse intensity surfaces in short range ordered ternary derivative structures based on ZnS, NaCl, CsCl and other structures. *Acta Cryst. A* **30**, 239-246.

Schmahl, W.W., Putnis, A., Salje, E., Freeman, P., Graeme-Barber, A., Jones, R., Singh, K.K., Blunt, J., Edwards, P.P., Loram, J. and Mirza, K. (1989). Twin formation and structural modulations in orthorhombic and tetragonal $YBa_2(Cu_{1-x}Co_x)_3O_{7-\delta}$. *Phil. Mag. Letts.* **60**, 241-248.

Shechtman, D., Blech, I., Gratias, D. and Cahn, J. W. (1984). Metallic phase with long-range orientational order and no translational symmetry. *Phys. Rev. Lett.* **53**, 1951-1953.

van Smaalen, S. (2007). *Incommensurate Crystallography*. IUCr Monographs on Crystallography 21, Oxford University Press, Oxford.

van Tendeloo, G., van Landuyt, J. and Amelinckx, S. (1976). The $\alpha \rightarrow \beta$ phase transition in quartz and aluminum phosphate as studied by electron microscopy and diffraction. *Phys. Stat. Sol. (a)* **33**, 723-735.

van Tendeloo, G. and Amelinckx, S. (1998). The origin of diffuse intensity in electron diffraction patterns. *Phase Transitions* **67**, 101-135.

Treacy, M.M.J., Gibson, J.M. and Howie, A. (1985). On elastic relaxation and long wavelength microstructures in spinodally decomposed indium gallium arsenide phosphide ($In_xGa_{1-x}As_yP_{1-y}$) epitaxial layers. *Phil. Mag. A* **51**, 389-417.

Ugarte, D. (1992). Curling and closure of graphitic networks under electron-beam irradiation. *Nature* **359**, 707-709.

Warren, B.E., Averbach, B.L. and Roberts, B.W. (1951). Atomic size effect in the X-ray scattering by alloys. *J. Appl. Phys.* **22**. 1493-1496.

Welberry, T.R. (1986). Multi-site correlations and the atomic size effect. *J. Appl. Cryst.* **19**, 382-389.

Welberry, T.R. (2004). The importance of multisite correlations in disordered structures. Ferroelectrics **305,** 117-122.

Welberry, T.R. and Butler, B.D. (1994). Interpretation of diffuse X-ray scattering *via* models of disorder. *J. Appl. Cryst.* **27**, 205-231.

Welberry, T. R., Withers, R. L. and Mayo, S. C (1995). A modulation wave approach to understanding the disordered structure of cubic stabilized zirconias (CSZs). *Journal of Solid State Chem.* **115**, 43-54.

Wilson, J.A., Di Salvo, F.J. and Mahajan, S (1975). Charge-density waves and superlattices in the metallic layered transition metal dichalcogenides. *Adv. In Phys.* **24**, 117-201.

Withers, R.L (2005). Disorder, structured diffuse scattering and the transmission electron microscope. *Z. für Kristallogr.* **220**, 1027-1034.

Withers, R.L., Ling, C.D. and Schmid, S (1999). Atomic modulation functions, periodic nodal surfaces and the three-dimensional incommensurately modulated $(1\text{-}x)Bi_2O_3.xNb_2O_5$, $0.06 < x < 0.23$, solid solution. *Z. für Kristallogr.* **214**, 296-304.

Withers, R.L., Otero-Diaz, L.C., Goméz-Herrero, A., Landa-Canovas, A.R., Prodan, A., van Midden, H.J.P. and Norén, L. (2005). As-As dimerization, Fermi surfaces and the anomalous elecctrical transport properties of UasSe and ThAsSe. *Journal of Solid State Chem.* **178**, 3159-3168.

Withers, R.L., Otero-Diaz, L.C. and Thompson, J.G. (1994a). A TEM study of defect ordering in a calcium yttrium sulfide solid solution with an average NaCl-type structure. *Journal of Solid State Chem.* **111**, 283-293.

Withers, R.L. and Liu, Y. (2005). Local crystal chemistry, structured diffuse scattering and inherently flexible framework structures. In: *Inorganic Chemistry Highlights II* (Eds. G.Meyer, D.Naumann & L.Wesermann), Wiley-VCH, 347-363.

Withers, R.L. and Schmid, S. (1994). A TEM and group theoretical study of α-PbO and its low temperature improper ferroelastic phase transition. *Journal of Solid State Chem.* **113**, 272-280.

Withers RL, Schmid S and Thompson JG. (1993). The tweed microstructure of α-PbO and its relationship to the low temperature improper ferroelastic phase transition. In *Defects and Processes in the Solid State: Geoscience Applications: The McLaren Volume*. J.N.Boland and J.D.Fitz Gerald, eds. Elsevier, Amsterdam, 305-316.

Withers, R.L., Thompson, J.G. and Welberry, T.R (1989). The structure and microstructure of α-Cristobalite and its relationship to β-Cristobalite. *Phys. Chem. Minerals* **16**, 517-523.

Withers, R.L., Thompson, J.G., Xiao, Y. and Kirkpatrick, R.J. (1994b). An electron diffraction study of the polymorphs of SiO_2 tridymite. *Phys. Chem. Minerals* **21**, 421-433.

Withers, R.L., Urones-Garrote, E. & Otero-Diaz, L.C. (2007). Structured diffuse scattering, local crystal chemistry and metal ion ordering in the (1-*x*)MgS.$^{x}/_{3}Yb_2S_3$, $0 \leq x \leq \sim 0.45$, 'defect' *NaCl* system. *Phil. Mag.* **87**, 2807-2813.

Withers, R.L.; Vincent, R. and Schoenes, J. (2004). A low temperature electron diffraction study of structural disorder and its relationship to the Kondo effect in ThAsSe. *Journal of Solid State Chem.* **177**, 701-708.

Withers, R.L., van Midden, H.J.P., Prodan, A.B., Midgley, P.A., Schoenes, J. and Vincent, R. (2006). As-As dimerization, Fermi surfaces and the anomalous transport properties of UAsSe and ThAsSe. *Journal of Solid State Chem.* **179**, 2190-2198.

Withers, R.L.; Welberry, T.R.; Brink, F.J. and Norén, L. (2003). Oxygen/fluorine ordering, structured diffuse scattering and the local crystal chemistry of $K_3MoO_3F_3$. Journal of Solid State Chem. **170**, 211-220.

de Wolff, P.M. (1974). The pseudo-symmetry of modulated crystal structures. *Acta Cryst. A* **30**, 777-785.

Yamamoto, A. (1982). Modulated structure of wüstite ($Fe_{1-x}O$). *Acta Crystallogr.B* **38**, 1451-1456.